Seasonal to decadal variability and persistence properties of the Euro-Atlantic jet streams characterized by complementary approaches

Hugo Banderier[1,2], Alexandre Tuel[3], Tim Woollings[4], and Olivia Martius[1,2,5]

[1]Institute of Geography, University of Bern, Bern, Switzerland
[2]Oeschger Center for Climate Change Research, University of Bern, Bern, Switzerland
[3]Galeio, Paris, France
[4]Atmospheric, Oceanic and Planetary Physics, University of Oxford, Oxford, United Kingdom
[5]Mobiliar Lab for Natural Risks, University of Bern, Bern, Switzerland

Correspondence: Hugo Banderier (hugo.banderier@unibe.ch)

Abstract. Recent studies have highlighted the link between upper-level jet stream dynamics, especially the persistence of certain jet configurations, and extreme summer weather in Europe. The weaker and more variable nature of the jets in summer makes it difficult to apply the tools developed to study them in winter, at least not without modifications. Here, to further investigate the link between jets and persistent summer weather, we present two complementary approaches to characterize the jet dynamics in the North Atlantic sector and use them primarily on the northern hemisphere summer circulation.

First, we apply the self-organizing map (SOM) clustering algorithm to create a 2D distance-preserving discrete feature space to the tropopause-level summer wind field over the North Atlantic. The dynamics of the tropopause-level summer wind can then be described by the time series of visited SOM clusters, in which a long stay in a given cluster relates to a persistent state and a transition between clusters that are far apart relates to a sudden considerable shift in the configuration of upper-level flow.

Second, we adapt and apply a jet core detection and tracking algorithm to extract individual jets and classify them into the canonical categories of eddy-driven and subtropical jets (EDJ and STJ, respectively). Then, we compute a wide range of jet indices on each jet category for the entire year to provide easily interpretable scalar time series representing upper-tropospheric dynamics.

This work will focus on the characterization of historical trends, seasonal cycles, and persistence properties of the jet stream dynamics, while ongoing and future work will use the tools presented here and apply them to the study of connections between jet dynamics and extreme weather.

The SOM allows the identification of specific summer jet configurations, each one representative of a large number of days in historical time series, whose frequency or persistence had increased or decreased in the last decades. Detecting and categorizing jets adds a layer of interpretability and precision to previously and newly defined jet properties, allowing for a finer characterization of their trends and seasonal signals.

Detecting jets on pressure levels of maximum wind speed at each grid point instead of on the dynamical tropopause is more reliable in summer, and finding wind-direction-aligned subsets of 0-contours in a normal wind shear field is a fast and robust way to extract jet cores. Using the SOM, we isolate persistent circulation patterns and assess if they occur more or

less frequently over time. Using properties of the jets, we confirm that the northern hemisphere summer subtropical jet is weakening, that both jets get wavier, and that they overlap less frequently over time. We find no significant trend in jet latitude or in jet persistence. Finally, both approaches agree on a rapid shift in subtropical jet position between early and late June.

1 Introduction

Extratropical tropopause-level jet streams are narrow bands of westerly winds and are one of the most prominent features of the upper-tropospheric circulation. Their large variability at daily time scale (Woollings et al., 2014) along with their link to extreme weather (e.g., Martius et al., 2006; Mahlstein et al., 2012; Harnik et al., 2014) makes them an important object of research in meteorology and atmospheric dynamics.

From a climatological perspective, jet streams are often separated into two categories based on their location and momentum source (Kållberg et al., 2005; Koch et al., 2006; Harnik et al., 2014; Winters et al., 2020; Spensberger et al., 2023). The subtropical jet (STJ) is located at the poleward edge of the Hadley cell. It draws its momentum from the thermally driven Hadley cell circulation and is mainly confined to high levels, typically between 400 and $150\,\mathrm{hPa}$ (Krishnamurti, 1961; Held and Hou, 1980). The eddy-driven jet (EDJ) can be found further poleward, inside the Ferrell cell. It is also referred to as the subpolar or extratropical jet. It is driven by momentum flux convergence associated with midlatitude synoptic eddies (Palmen and Newton, 1948; Held, 1975; Schneider, 1977; Woollings et al., 2010). It has a much deeper vertical extent, typically extending below $700\,\mathrm{hPa}$. The separation into STJ and EDJ is not always clear, as both sources of momentum are often present to varying degrees to drive either jets and depend on each other (Lee and Kim, 2003; Martius, 2014).

Certain features and configurations of the jet have received particular attention over the last years due to their links to other aspects of the circulation, surface weather, or both. The latitude of the low-level EDJ has been identified as a major mode of variability of the wintertime Atlantic circulation (Athanasiadis et al., 2010; Woollings et al., 2010; Hannachi et al., 2012). A very zonal (low tilt) EDJ paired with a north-shifted STJ can create a rare but very persistent circulation pattern with a merged jet (Harnik et al., 2014). An instantaneously meandering jet is the marker of Rossby waves (e.g. Vallis, 2017), but strong narrow jets can act as waveguides for them too (Hoskins and Ambrizzi, 1993; Martius et al., 2010; Wirth, 2020; White, 2024). A locally sinuous jet may also mark the presence of a block (e.g. Nakamura and Huang, 2018; Woollings et al., 2018b). Jet properties also interact with each other. For instance, in winter, the EDJ's latitude influences its persistence and predictability (Franzke and Woollings, 2011; Barnes and Hartmann, 2011), and a jet with low speed has a higher daily variability in its waviness and latitude (Woollings et al., 2018a), which is hypothesized to favor blocks. Jet properties have also been linked to extreme events. The position of the EDJ modulates the odds of extreme events in the midlatitudes (Mahlstein et al., 2012), and so does its waviness (Röthlisberger et al., 2016b; Jain and Flannigan, 2021). Over Eurasia, the persistent simultaneous presence of the EDJ and STJ is associated with increased odds of extreme heat in summer in certain regions of western Europe (Rousi et al., 2022). Recently, statistical models trained on timeseries of a few (5-10) wintertime EDJ properties (introduced by Barriopedro et al., 2022) were used to skillfully predict air stagnation (Maddison et al., 2023) and temperature extremes (García-Burgos et al., 2023).

Climate change is expected to affect the jet streams in several ways. Through connections highlighted in the previous paragraph, themselves potentially affected by climate change, trends in jet stream properties may translate into trends in various aspects of atmospheric circulation and surface weather (e.g. Held, 1993; Stendel et al., 2021). The poleward shift of the jet streams under climate change was hypothesised very early on (e.g. Held, 1993). It is now observed in historical data in the global mean, albeit more clearly in winter than in summer, and mostly for the EDJ. However, the signal is weak in the North Atlantic sector (Woollings et al., 2023). This poleward shift is projected to continue in future simulations (Barnes and Polvani, 2013; Lachmy, 2022; Woollings et al., 2023). For the STJ, the historical trend is season- and region-dependent. For the North Atlantic sector, Totz et al. (2018) report a poleward trend in the transition seasons and an equatorward trend in summer. The North Atlantic STJ is also weakening with time, especially in summer (Woollings et al., 2023; D'Andrea et al., 2024), and so is the North Atlantic EDJ in the last two decades (Francis and Vavrus, 2012; Woollings et al., 2018a), although an opposite trend has been observed for longer time periods (Blackport and Fyfe, 2022). In future simulations, a positive trend is projected for the maximum speed of the EDJ core, although this signal is not yet apparent in historical data (Shaw and Miyawaki, 2024). In past data and using three different metrics, Francis and Vavrus (2015), Di Capua and Coumou (2016), and Martin (2021) all find slight increases in EDJ waviness, but a stable STJ waviness in the last cited paper. Further downstream however, Lin et al. (2024) find an increase in waviness for the Asian Jet that has an Atlantic origin. By contrast to past trends, for future winters, Peings et al. (2018) find a decrease in waviness accompanied by a strengthening and squeezing of the EDJ. This opposite trend in EDJ waviness for past and future data is consistent with the findings of Cattiaux et al. (2016), who find a slight increase in waviness in the past only for certain basins (including the North Atlantic) and seasons, but an overall decrease in waviness in future simulations. The conflicting results in jet meandering depending on the period and metric chosen were highlighted by Blackport and Screen (2020) and overall remain a subject of discussion in the community (Geen et al., 2023).

Most of the current research in atmospheric science requires reducing the complexity of the circulation from time-varying 2D or 3D fields to a smaller feature space. These simplified feature spaces are either continuous, like jet indices (Woollings et al., 2010; Di Capua and Coumou, 2016; Barriopedro et al., 2022) or the projection of instantaneous fields on principal components, or discrete, like weather regimes (e.g., Michelangeli et al., 1995) or other types of clustering methods like the self-organizing map (SOM; Gibson et al., 2017; Weiland et al., 2021; Rousi et al., 2022; Stryhal and Plavcová, 2023). These methods can also be categorised based on the number of choices the user needs to make, from statistical, e.g. dimensionality reduction or clustering, to expert-defined, e.g. jet indices, blocking indices or wave breaking indices. Statistical approaches are typically less fallible since they require fewer choices, but tend to be harder to interpret than expert-defined features. Certain statistical methods are also known to produce physically unrealistic patterns that can lead to wrong interpretations (Monahan and Fyfe, 2006).

Here, and to lay the groundwork for further research on all the interactions between jet streams and other large-scale circulation features or surface weather events, we develop two complementary diagnostic tools for the jet streams. Using two methods allows us to view the circulation from different angles, and to combine the strengths of statistical and expert-defined approaches. Recently, Madonna et al. (2017) recommended the use of different, complementary, and problem-dependent approaches to describe the jet streams. Both of the diagnostic tools presented in this work are adaptations of existing techniques

widely used in the field of atmospheric sciences, with implementation details changed and tailored for the specific needs of summertime, upper-level circulation.

The first one is the self-organizing map, a clustering algorithm. The SOM creates a distance-preserving discrete feature space that makes it a valuable tool to study stationarity and recurrence (Tuel and Martius, 2023), a major factor in extreme events. The second one is a set of jet characteristics computed on individual jet cores that are extracted, tracked, and categorized from wind fields. This provides a collection of continuous interpretable time series representing the jets over time.

After presenting both techniques in detail, we demonstrate their capabilities on reanalysis data. This work focuses more on summer than the rest of the year. This season receives less attention when designing methods to characterize the circulation, and is yet very important for extreme events and which presents interesting, different trends compared to the rest of the year (Harvey et al., 2023). The SOM will only be trained on June, July and August (JJA) days, but the jets are detected on year-round data to provide more context to the JJA results.

The seasonal varability of the upper level circulation is characterized using both the week-by-week mean pathway through the SOM and the seasonal cycle of the jet properties, and interannual trends are assessed for state occurence frequencies as well as for individual jet properties such as jet waviness. The SOM approach is related to the more established weather regimes, as their connections to weather impacts have been thoroughly studied. Finally, the persistence of the upper level flow, characterized using both state persistence using the SOM, and feature lifetime using jet tracking, is quantified. These preliminary results are in preparation for future work delving deeper into the comparison between these two, sometimes diverging, notions of persistence.

2 Data and Methods

2.1 Data

We use 6-hourly gridded fields for the 1959-2022 period, over the $80\,°\mathrm{W} - 40\,°\mathrm{E}$, $15\,°\mathrm{N} - 80\,°\mathrm{N}$ domain, extracted from the European Centre for Medium-Range Weather Forecasts reanalysis version 5 (hereafter, ERA5 reanalysis; Hersbach et al., 2020). The main variables we use are the horizontal wind components u and v, and the wind speed $U = \sqrt{u^2 + v^2}$, on the six following pressure levels: 175, 200, 225, 250, 300 and $350\,\mathrm{hPa}$.

Both algorithms take as input, at each timestep, 2D (longitude-latitude) fields of upper-tropospheric wind. We flatten the three wind fields (u, v and U) in the vertical by retaining, at every grid point, their value at the pressure level where U is maximal since our goal is to detect jet cores, and they are defined as local wind speed maxima. We keep track, in a separate 2D field, of that pressure level, to use later in the jet categorization. Both methods then add different preprocessing steps to this vertical maxima data, which will be discussed in the relevant sections.

We additionally use the potential temperature on the surface of maximum wind speed, and the horizontal wind speed magnitude at the $500\,\mathrm{hPa}$ pressure level. Finally, summer Euro-Atlantic weather regimes (Cassou et al., 2005; Grams et al., 2017) are computed from $500\,\mathrm{hPa}$ geopotential height anomalies from ERA5, computed relative to a daily climatology including all years from 1959 to 2022, smoothed with a 15-day centered rolling window.

2.2 SOM clustering

2.2.1 Definition

The self-organizing map (SOM) is a clustering method first introduced by Kohonen (1982) (see also Kohonen, 2013, for an in-depth review), whose main appeal over simpler predecessors like k-means is the creation of a 2D distance-preserving discrete feature space. The SOM may be presented as a modification of k-means. In k-means, data points are split in k groups called clusters, such that the variance within the clusters is minimal and the variance between clusters is maximal. Each cluster is then represented by the mean of all its members, called the cluster center or sometimes weights matrix. The SOM adds another layer to this algorithm, by placing the clusters on the nodes of a regular 2D grid of size $k = n \times m$, typically rectangular or hexagonal, and has a distance metric on this discrete space, for example the Euclidean distance between nodes. There, a cluster i is defined by its weights matrix $\mathbf{w}_i$ which is not equal in general to its center, but rather the result of a training process during which clusters on neighboring nodes have an influence modulated by the distance between nodes. Hereafter, we conflate the clusters and the nodes they sit on, and the phrases "distance between clusters" and "neighboring clusters" are to be understood as, respectively, "distance between the nodes on which the clusters sit" and "clusters on neighboring nodes".

The training then has a similar objective as k-means, with the additional constraint that a pair of neighboring clusters should be more similar to each other than a pair of distant clusters. This constraint ensures the distance-preserving property of the created phase space. The desired similarity of neighboring clusters may be enforced by the choice of an appropriate neighborhood function. The neighborhood function, typically a Gaussian, is a parametric function with parameter σ, the neighborhood radius, and is applied to the distance between clusters in the training process. The convergence of the algorithm relies on decreasing σ, equivalent in our case to the Gaussian's scale parameter, over time during the training. However, the initial and final σ values as well as the decay function are additional choices that need to be made. In general, a larger σ allows for more similar neighbours, and the limiting case $\sigma \to 0$ is equivalent to k-means.

Both the SOM and k-means share the same challenge, that is the choice of the number of clusters k. The SOM further adds the choice of the shape of the grid, $k = n \times m$.

Allowing neighboring clusters to be similar can lead the SOM to be a worse clustering algorithm, in the usual sense of cluster separation, than k-means, if the neighborhood radius is different from zero at the end of training (Gibson et al., 2017). Its strength resides in the creation of a distance-preserving feature space. One of the reasons we use SOM is the interpretability of the trajectory when expressed as a succession of cluster visits. Once the SOM is trained, each timestep is assigned to a cluster, its "best matching unit" or BMU, defined as $\mathrm{BMU}(t) = \mathrm{argmin}_i \|\mathbf{x}_t - \mathbf{w}_i\|$ with $\mathbf{x}_t$ the wind field at timestep t. Thus, the input time series is represented as a succession of *stays* in clusters and *jumps* between clusters, where long *stays* or short *jumps* point to persistence, and long *jumps* indicate abrupt changes in the configuration of the upper-level flow.

2.2.2 Specific implementation

For the SOM algorithm, the June-July-August (JJA) vertically maximum wind speed field (see Data) is coarsened to a $1.5\,^\circ$ resolution grid to reduce the computational complexity and to focus on the larger scale features. However, the final results are

shown at the initial $0.5\,^\circ$ resolution. This is done by representing clusters with their centers, computed with the original higher resolution data, rather than their weights.

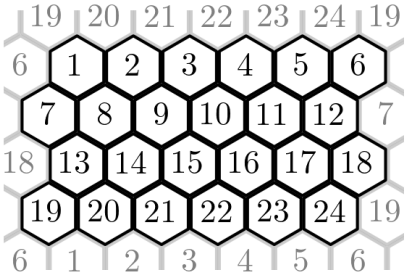

Figure 1. Hexagonal topology SOM with ideal grid size. The SOM clusters are in black and the grayed clusters illustrate the periodic boundaries.

The grid (of size $n \times m$) is hexagonal with periodic boundary conditions, and is associated with a discrete distance metric. As a consequence, clusters are at a unit distance away from their nearest neighbors, and the bottom row and left column are at a unit distance away from the top row and right column, respectively (see figure 1), such that each and every cluster has six neighbors, all at a unit distance. Periodic boundary conditions were chosen to avoid creating an artificial over representation of the central clusters, which would have diminished the relevance of our persistence measures later on. The SOM is initialized using the first two principal components of the input data to ensure reproducibility, as recommended in Kohonen (2013). Before training, the data is standardized and weighted by the cosine of latitude. We use the single batch training algorithm (Kohonen, 2013), repeated 50 times with the neighborhood radius σ exponentially decaying from 2 to 0.2. This training algorithm does not involve a learning rate.

To inform our decision on the SOM grid size, we use two performance metrics of the SOM. The first one is the energy function E of the SOM based on Heskes (1999) (see eq. 1), and the second one is the 5$^{\text{th}}$ percentile of the projection of data points on their BMUs, defined as P in eq. 2. These metrics are a function of the ensemble of SOM weights $W = \{\mathbf{w}_i, 1 \leq i \leq n \times m\}$, the ensemble of input data vectors $\mathbf{x} \in X$, of size N, as well as the topological properties of the SOM. The grid distance between two SOM clusters i and j is precomputed and stored in a matrix of elements d_{ij}. These distances are then transformed by the neighborhood function to obtain the pairwise neighborhood parameters $h_{ij} = f(d_{ij}; \sigma)$ based on the SOM's neighborhood radius σ. In this work, f is a zero-mean Gaussian with scale parameter σ.

$$E(W) = \frac{1}{N} \sum_{\mathbf{x} \in X} \min_{1 \leq i \leq n \times m} \sum_{j=1}^{n \times m} h_{ij} \|\mathbf{x} - \mathbf{w}_j\|^2 \tag{1}$$

$$P(W) = \underset{\mathbf{x} \in X}{Q_5} \left(\max_{1 \leq i \leq n \times m} \frac{\mathbf{x} \cdot \mathbf{w}_i}{\|\mathbf{x}\| \|\mathbf{w}_i\|} \right) \tag{2}$$

The goal is to minimize E and maximize P while maintaining a reasonably low number of clusters. The E and P objectives are similar, but the latter allows one to explicitly limit how poor the poorest projections on the SOM clusters are, making sure that most days are well-described in the 2D feature space described by the SOM since current and future work includes working on extreme configurations of the upper-level circulation. Testing for many sizes ranging from 4×4 to 9×9 was performed, and the chosen size is 6×4.

2.2.3 SOM metrics

We compute statistical properties from the trained SOM, including the populations of each cluster and their annual trends, two quality metrics as well as the average and maximum residence time in a given cluster.

The first SOM metric of note is an analogue to the persistence index in dynamical systems theory. The average residence time at a given cluster i is simply given by the average length of time during which $\mathrm{BMU}(t) = i$, starting at the transition from another cluster to i. The definition can be loosened to the length of time during which $\mathrm{BMU}(t)$ remains within a given distance of i. With a large SOM, that sometimes features minute differences between neighboring clusters, this second definition with a small distance can be a more realistic measure of persistence. To account for varying degrees of similarity between neighboring clusters, we do not use the discrete grid distance between clusters but instead the Euclidean distance between SOM cluster weight matrices. At the start of JJA, the first stay starts on the first populated cluster, i_0. The stay continues if $\mathrm{BMU}(t)$ is on i_0 or any other cluster whose weight matrix has a distance from i_0 that is within the 10^{th} percentile of inter-cluster-weight distances. When $\mathrm{BMU}(t)$ no longer respects this condition, a new stay begins at a new cluster i_1. The stay is associated to the most visited cluster during the stay, which is not necessarily the starting one.

We provide two cluster-wise quality metrics. The first one is the root mean square error (RMSE), defined for each cluster as the mean Euclidean distance between its weight matrix and its members. A low RMSE is preferred. The second quality metric is the cluster separatedness. We compute, for each pair of clusters, the ratio of the Euclidean distances between their weight matrix to the grid distance that separates them. We then average all the ratios for all the pairs containing cluster i to obtain cluster i's separatedness. A high separatedness is preferred.

Finally, we will relate our SOM clustering to the summer Euro-Atlantic weather regimes. Following Grams et al. (2017) but using only four weather regimes, we assign to each day of summer one of four weather regimes if the associated weather regime index is bigger than that of the three other regimes for at least 5 consecutive days and is above its temporal standard deviation within this time span. With this definition, $40\ \%$ of the timesteps are not assigned to any weather regime. We then count the number of timesteps previously assigned to a SOM cluster that are now also assigned to a weather regime.

2.3 Feature detection and tracking

The SOM is a powerful clustering tool to characterize the circulation as a whole in a given region. However, one might want to know more specific information about some of the components of the circulation, expressed as numbers rather than features on a composite map. We now turn to the methods we use to detect jets in vertical maximum 2D wind fields, to separate them into broad categories, to track them over time to assess their lifetime and evolution, and finally to extract a wide range

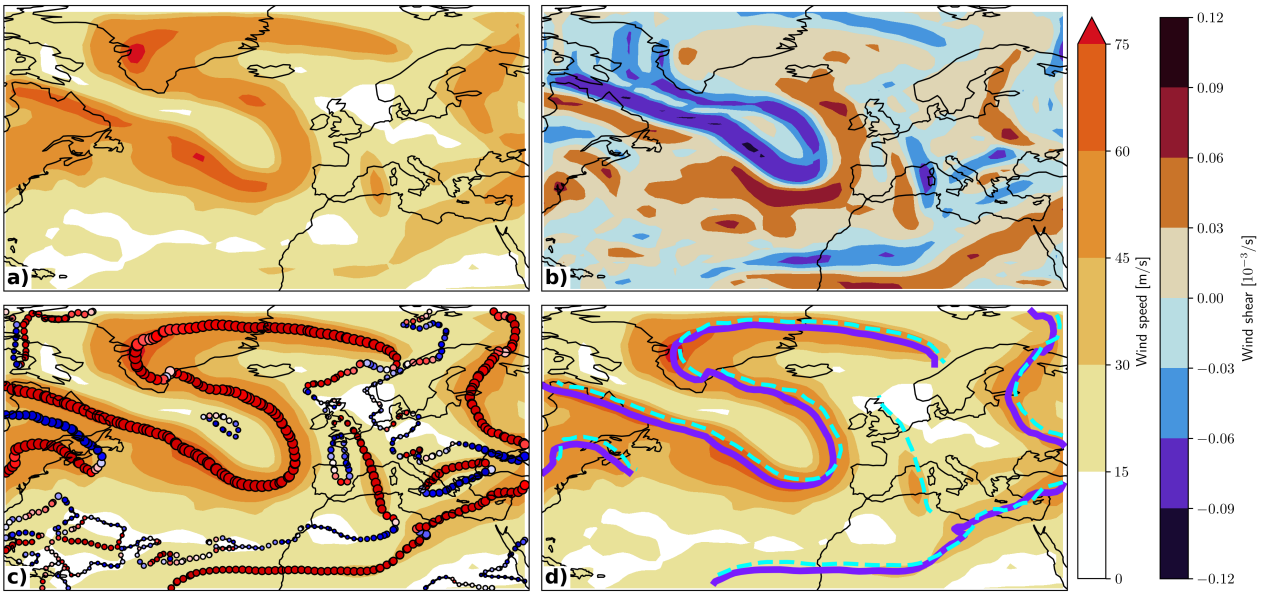

Figure 2. Results of our jet detection algorithm for 0000 UTC 9 Oct 1959. a) The smoothed, vertical maximum wind speed [m/s] field given as input to the algorithm. b) The smoothed horizontal normal wind shear on the same 2D surface. c) The $\tau = 0$ contours where the size of the points corresponds to the wind speed field, and the color corresponds to the alignment with the horizontal wind vector field from blue (close to -1) to red (close to $+1$). d) The jets extracted from contours, as solid purple lines. The output of the S17 algorithm is represented as dashed cyan lines for comparison.

of properties out of them. Thanks to seasonally-varying thresholds (see next section), our method works equally well across the year. Therefore, we apply it to the full dataset rather than only to JJA, which will allow us to broaden the discussion of inter-annual trends to other seasons and paint a full picture of the jets' annual cycles.

2.3.1 Jet detection

Our jet detection algorithm is an adapted version of the method by Spensberger et al. (2017, hereafter S17). It can be applied to each timestep independently, allowing for parallelization.

The vertical maximum wind speed fields (u, v and U; see Data) are coarsened to a grid of $1.5\,°$. Our choice of 2D fields, the level of maximum wind speed over several pressure levels, as described in Data, is the first difference to S17, who used wind fields interpolated onto the 2 PVU surface, where 1 PVU = $10^{-6}\mathrm{Kkg}^{-1}\mathrm{m}^2\mathrm{s}^{-1}$. Internal testing has shown that the STJ is often undetectable on the 2 PVU surface in JJA, while it clearly appears on our 2D fields. The main criterion used to find jets is the horizontal normal wind shear $\tau := \frac{\partial U}{\partial n} = \frac{v}{U}\frac{\partial U}{\partial x} - \frac{u}{U}\frac{\partial U}{\partial y}$. Following Berry et al. (2007), $\tau = 0$ is a necessary condition for a jet. The first step of this algorithm is thus to find contours of $\tau = 0$, using a contour detection routine.

The points along the contours are filtered using a wind speed and an alignment threshold. We use as wind speed threshold the day-of-year climatological 75$^{\text{th}}$ percentile of 6-hourly wind speed, so that the algorithm works equally well in all seasons. The

contour must also be aligned with the wind speed. This is done by computing the local tangent vector $\mathbf{t} = \frac{\mathrm{d}\mathbf{x}}{\mathrm{d}s}$, with s the linear path coordinate, and computing the alignment dot product $a = \frac{\mathbf{t}}{\|\mathbf{t}\|} \cdot \frac{\mathbf{u}}{U}$, as done in Molnos et al. (2017). We require $a > 0.3$ for a jet. With very few values of a different from either -1 or $+1$, the performance of the algorithm is largely insensitive to the exact value of this threshold.

Jets are defined as series of consecutive potential jet points, i.e. points in the contours that follow the two point-wise criteria defined in the previous paragraph. We allow series to contain small stretches of one to three points that do not respect the thresholds if they are surrounded by points that do. The series need to verify one additional criterion to be finally accepted as jets. The path integral of the wind speed along the path of the series is computed using a method detailed in section 2.3.2 and is compared against a day-of-year-varying threshold, heuristically constructed from the wind speed threshold U^*, the radius of the Earth R and the longitudinal extent of the domain $\Delta\Lambda$ as $U^* R \Delta\Lambda \cos(45°)/3$.

Each jet J_a of length L_a is represented as a sequence of L_a points $k = 1 \dots L_a$, themselves a collection of coordinates with longitude λ_a^k, latitude ϕ_a^k, pressure p_a^k level, along with additional point-wise properties that can be of use to derive jet properties, e.g. the u_a^k or v_a^k components of wind or the wind speed U_a^k.

Figure 2 demonstrates the jet detection algorithm in four steps and compares its results against the original S17 algorithm, but applied to the same 2D data to ignore the potential problems raised by the 2 PVU surface in this basin. The algorithms produce similar results with a few disagreements that can be explained by studying the differences between our algorithm and S17. Our algorithm finds 0-contours of τ rather than low values of $\frac{\mathrm{d}(\tau U)}{\mathrm{d}n}$, extracts jets as subsets of contours using an alignment criteria instead of connecting points using a shortest-path algorithm. These two differences seem to help find jet cores closer to the local wind maxima, a problem that was highlighted in the original work. Furthermore, by allowing jets to not respect the two local criteria (speed and alignment) for up to three points, our algorithm is more likely to find one long jet rather than several shorter pieces. This latter point is sometimes a problem when an EDJ and a STJ are detected as one long single jet. However, this does not happen often in 6-hourly data, and it is typically accompanied by an abrupt change in pressure level, wind speed, or alignment along the jet core, which helps to highlight and resolve these cases. This issue is not solved systematically in the current version of the algorithm, but might come in a later version.

2.3.2 Jet properties

Introduced by Woollings et al. (2010), the Jet Latitude Index (JLI) measures the latitude of maximum wind speed in the profile obtained by averaging the wind speed field at low altitudes, to filter out the STJ and only capture the EDJ, in a longitudinal band, originally $60\,°\mathrm{W} - 0\,°\mathrm{E}$, the North Atlantic basin. It is often used in combination with the Jet Speed Index (JSI), the maximum wind speed used to find the JLI. These simple and highly interpretable metrics have been used to describe EDJ variability at timescales ranging from daily to multi-decadal (Woollings et al., 2014, 2018a).

Over time, several other similarly simple yet powerful jet indices have been developed to describe the jet stream in a simplified way, or to link it to other phenomena. Such indices include the zonal jet index (Harnik et al., 2014), several sinuosity/waviness metrics (Francis and Vavrus, 2015; Di Capua and Coumou, 2016; Cattiaux et al., 2016; Röthlisberger et al., 2016a; Huang and Nakamura, 2016) linked to extreme events and persistence (Röthlisberger et al., 2016b; Martin and Norton, 2023),

up to a ten-index toolbox (Barriopedro et al., 2022) that has been used for skillful predictions of cold and hot spells in Europe (Maddison et al., 2023).

In the presence of several jets, many of these indices give an incomplete or improper picture. Using our jet core detection algorithm (section 2.3.1), all the jet indices can be computed for each jet individually. The details of computations and potential differences with the original metrics are explained in the following paragraphs.

In the previous section 2.3.1 we mentioned point-wise jet properties storing each point's position and wind speed. The mean of these point-wise jet properties constitute the first jet properties we compute. The ones of interest correspond to the mean position of the jet. The properties `mean_lon`, `mean_lat` and `mean_lev` are all computed as weighted averages of the longitude λ, the latitude ϕ and the pressure level p respectively, using the point-wise wind speed values U_a^k as weights. In the spirit of the JLI, the maximum wind speed is found and stored as `spe_star`. The position on the (lon-lat) plane of this maximum is stored as `lon_star` and `lat_star`.

A path integral of the wind speed along the jet core and using the haversine distance is performed and stored as `jet_int`. Explicitly, the integral $\int U \mathrm{d}s$ is discretized using central finite differences and computed with a discretized approximation of

$$\mathrm{d}s = 2R \arcsin \sqrt{\sin^2\left(\frac{\mathrm{d}\phi}{2}\right) \cdot \cos^2\left(\frac{\mathrm{d}\lambda}{2}\right) + \cos^2(\phi) \cdot \sin^2\left(\frac{\mathrm{d}\lambda}{2}\right)}$$

with $R = 6.378 \times 10^6\,\mathrm{m}$ the radius of the Earth. This integral is performed once more over a smaller domain ($\lambda > 10\,^\circ\mathrm{W}$) and stored as `int_over_europe`.

To obtain the local width of the jet a at a point k along its core, normal segments are drawn in continuous space on either side of the jet core, of length 10° each. Along each segment, the wind speed is interpolated from the gridded wind speed field. For each segment, the haversine distance between the core and the first point to have a wind speed below $0.75 \times U_a^k$ represents the local width of the jet on this side, and the full local width is the sum of the local widths computed on either side. In some cases, only one segment can be drawn if the jet core is too close to a boundary. In this case, the local width is simply twice the width computed on the only valid side. The local widths w_a^k are computed on every jet core point, and then averaged, with U_a^k as weights, to finally obtain the jet's mean `width`.

The tilt of the jet is computed as the slope of a U_a^k-weighted linear fit of the ϕ_a^k against the λ_a^k. The linear coefficient is stored as `tilt`, while the intercept is discarded. The quality of this linear fit, the R^2 value, is used to compute a natural measure of jet waviness: $\texttt{waviness1} = 1 - R^2$. Another natural way of characterizing waviness from jet cores is the U_a^k-weighted average distance between ϕ_a^k and `mean_lat`, stored as `waviness2`. For short jets, the difference between the tilt and the waviness is hard to assess, and in this case `waviness1` will not capture waviness well. However, if a jet is both tilted and wavy, only `waviness1` will be able to separate these properties. These two waviness metrics are compared against adaptations of waviness metrics found in the recent literature. `wavinessFV15`, adapted from Francis and Vavrus (2015), is computed as the U_a^k-weighted average of the local meridional circulation index: $\mathrm{MCI}_a^k = \frac{(v_a^k - \overline{v_a})|v_a^k|}{(U_a^k)^2}$. `wavinessDC16`, adapted from Di Capua and Coumou (2016), is computed as the ratio between the haversine-integrated length of the jet ($\int 1 \mathrm{d}s$) to the length of the circle arc $\overline{\phi} \cdot R \cdot \Delta\lambda_a$, where $\overline{\phi}$ is `mean_lat` and $\Delta\lambda_a$ is the extent of the jet in longitude expressed in radians. Finally,

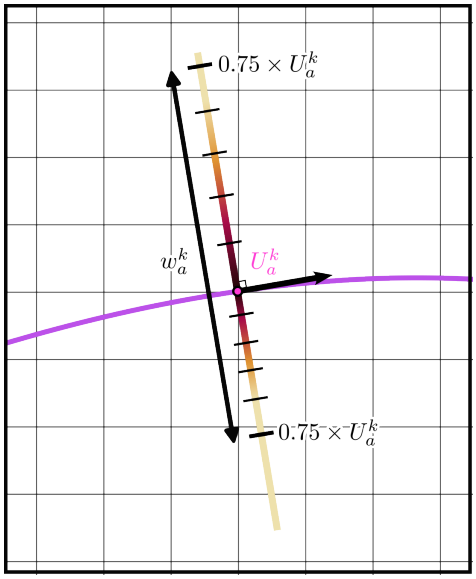

Figure 3. Schematic representing the local width computation, along a jet core a drawn in purple, for a single point k. In the schematic, the wind speed interpolated onto the half-segments is represented using a color gradient from black (core wind speed at the point of interest, U_a^k) to yellow (three quarters of local jet core wind speed, $0.75 \times U_a^k$) with a tick every $0.05 \times U_a^k$. The schematic, especially the grid spacing, is not to scale.

`wavinessR16`, adapted from Röthlisberger et al. (2016a), is computed as the sum of absolute differences in latitudes between neighbors $|\phi_a^{k+1} - \phi_a^k|$, divided by the sum of differences in longitudes.

An index that can be computed that will not be categorized per jet is the double jet index. From the found jets, a 2D (time-lon) binary array is built, where an element is set to `True` if at least 2 jets can be found at this timestep and longitudinal band over all latitudes and one hemisphere. The index is the zonal average of this array for longitudes over Europe, $10\,°\mathrm{W} < \lambda < 40\,°\mathrm{E}$.

In section 2.3.4, tracking the jets allows us to determine the lifetime of a jet object, as well as the instantaneous speed of the jet's center of mass.

2.3.3 Jet categorization

While some literature sees the types of jets highlighted in the introduction as regimes of a singular jet stream (Harnik et al., 2014, 2016), this work benefits from seeing them as categories one may assign to the previously detected jets. In instantaneous data, one cannot distinguish the jet from the eddies potentially driving it, since the quantification of the eddy momentum flux requires temporal filtering and averaging (e.g. Lachmy, 2022). One may instead rely on the vertical extent or baroclinicity of the jet, which is sometimes misleading due to the many factors influencing low-level winds, latitude, which is not sufficient on its own for global data (Winters and Martin, 2017), or potentially other metrics like vertical shear (Martius et al., 2010) or the height of the tropopause above the jet core. A recent, promising approach to establish this categorization bins the jets on the

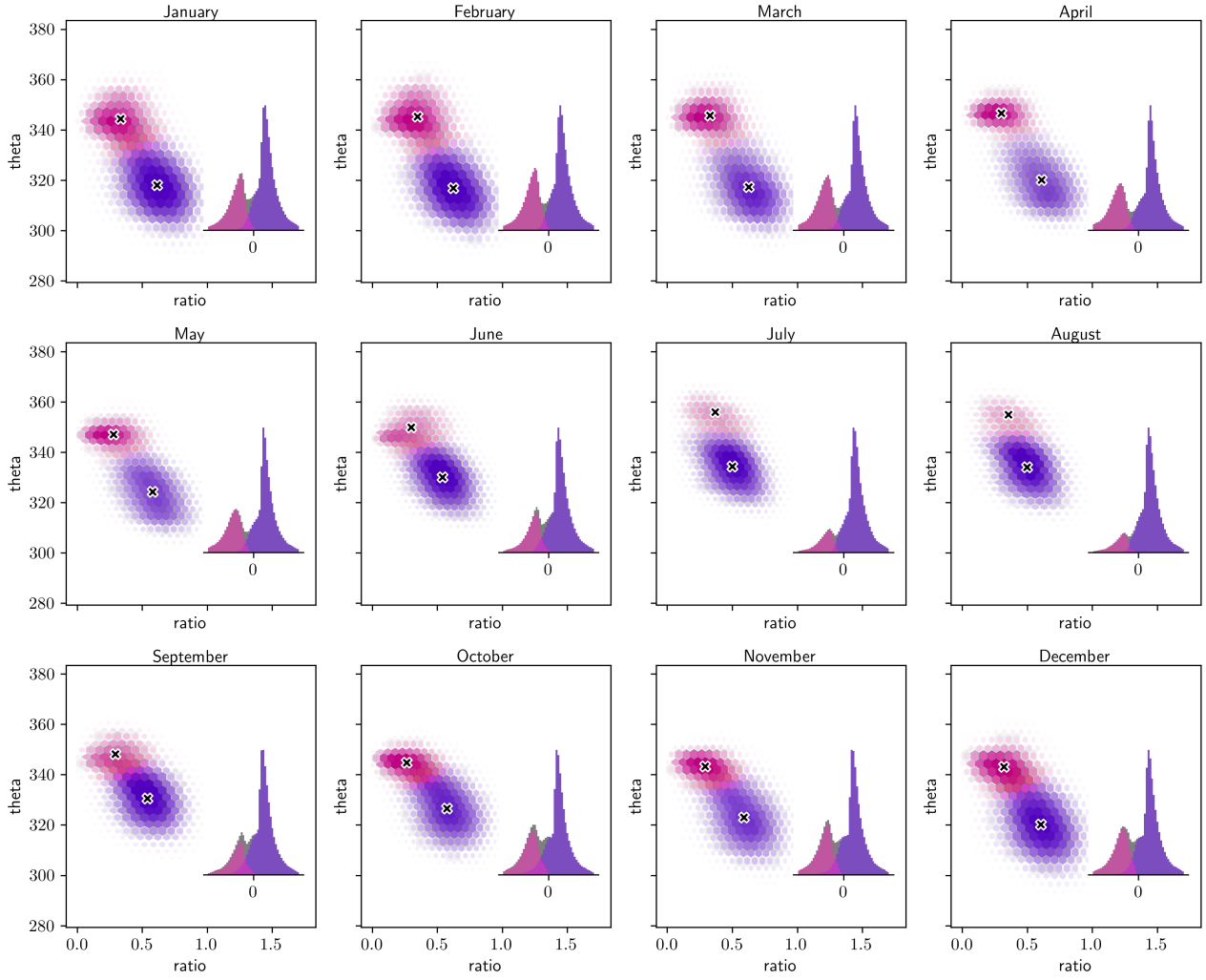

Figure 4. Demonstration of the jet categorization for each month of the year. The jet points are binned in the 2D space (baroclinicity proxy — potential temperature), in order to illustrate the underlying distribution in this 2D space. The size and lightness of each hexagon illustrate its height, while its color indicates the mean Gaussian assignment score, from pink (0 score, close to STJ component) to purple (1 score, close to EDJ component). The crosses indicate the center of each Gaussian, x_1 and x_2. On the lower right corner of each box, the quantity $\log \frac{\|x-x_1\|}{\|x-x_2\|}$ is binned, where x is a 2D vector containing a jet point's vertical extent proxy and potential temperature, and $\|y\|$ is the 2-norm of the vector y. This quantity is not the final score but serves illustrative purposes. The final score is averaged for each bin and indicated with the color of each bar, as for the hexagons.

2D feature space (Wind speed — Potential Temperature). The algorithm then extracts regions of high occurrences for oceanic basins across the world and for the whole year. The approach always finds two distinct regions that may be labeled STJ and EDJ, except for the North Atlantic basin in JJA (Spensberger et al., 2023, see their supplementary material for JJA).

A very similar approach is used here, but with another feature space to better highlight the weak but still present bimodality in jet property distribution in this basin and season. Our version of the algorithm uses the (baroclinicity – potential temperature) 2D phase space and fits a two-component Gaussian Mixture model to facilitate the discovery of the two regions. The baroclinicity or vertical extent proxy is similar to that used by Koch et al. (2006), and is defined as the ratio of low level ($500\,\mathrm{hPa}$) horizontal wind speed magnitude at the horizontal position of the jet point and the jet core speed itself. The illustration of this binning can be seen on figure 4, where the count of jet points in each hexagonal bin is represented by its lightness and size.

A two-component Gaussian mixture model assumes that the data are bimodal and tries to fit their empirical distribution as a sum of two Gaussian distributions. Each Gaussian is defined by a mean and covariance matrix that are fitted to the data. The model is fitted independently for each month to accommodate the large seasonal variation in the STJ's occurence frequency. The density in the EDJ Gaussian component at each point, computed using the standardized distance to this component's center, is then used as a continuous score and not a hard assignment. The EDJ component is identified as the component with lower potential temperature. Most jet points will have a score close to 0 (STJ point) or close to 1 (EDJ point), but some points lie inbetween and can be thought of as hybrid. The jets as a whole are assigned a category based on the mean of the scores of the points that constitute them.

The nature of this potential hybrid jet category is discussed in Appendix A. In short, it has an almost identical seasonal cycle to that of the STJ and is almost only present in JJA. Our final decision was therefore to carry on with only two categories, with a categorization cutoff informed by the distribution of EDJ component mean score.

2.3.4 Jet tracking

A straightforward object tracking algorithm is presented in this section. The program will assign a flag n to each jet at each timesteps, where the flag is carried over from a jet in a timestep to a jet in the next one according to a distance threshold.

The algorithm starts by assigning each jet in the first timestep a unique flag $1, 2, 3\ldots$. It then iterates over all timesteps t. For all flags that have appeared at least once in the previous four timesteps ($t-1$, $t-2$, $t-3$, $t-4$, i.e. a day with a time resolution of 6 hours), the algorithm extracts the most recent jet with this flag into a list of potential parents. This allows for jets to disappear for a few timesteps and mitigates the issue of short jets blinking in and out of the jet integral threshold from section 2.3.1. The potential children are all the jets present in the current timestep. For all pairs of a potential parent jet a and a child jet b, an overlap measure $o_{a,b}$ as well as a vertical distance $\delta_{a,b}$ are computed as described in equations 3 and 4.

$$o_{a,b} = \frac{|\Lambda_a \cap \Lambda_b|}{2}\left(\frac{1}{L_a} + \frac{1}{L_b}\right) \tag{3}$$

$$\delta_{a,b} = \frac{1}{|\Lambda_a \cap \Lambda_b|}\sum_{k,l:\lambda_k=\lambda_l}^{L_a,L_b} |\phi_l - \phi_l| \tag{4}$$

Where Λ_a is the ensemble of longitudes in jet a.

Both overlap and vertical distance metrics need to satisfy a certain threshold, respectively 0.5 and 10°. If both are met, the jets match and the child jet is assigned the parent's flag. If a child matches no potential parent, it is assigned a new flag, the

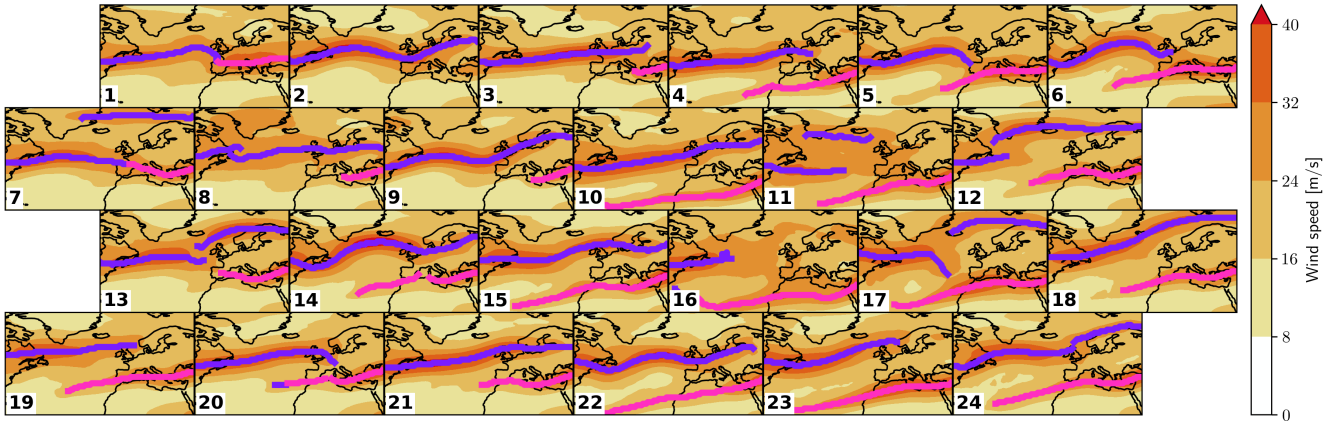

Figure 5. SOM training results on JJA wind speed fields. Composites of horizontal wind speed for all days corresponding to a cluster, and result of the jet core detection algorithm applied to the composite wind fields overlayed as colored lines; pink for STJ and purple for EDJ. The SOM cluster number is indicated by a number in the bottom left corner.

latest assigned flag plus one. If a child has two potential parents fulfilling both criteria, or if a parent has two children fulfilling them, the winner is the most recent one, and if both are as recent then it is the longest.

Using this, it is possible to infer the lifetime of a jet from its genesis to its decay, as well as to track the speed of its center of mass (COM), in $\mathrm{m/s}$ using the haversine distance between two 6-hourly-timesteps. The first use of these new jet properties is to filter out jets with 1- or 2-timestep lifetimes to filter out residual noise. The lifetime and (the inverse of the) COM speed can be seen as additional measures of persistence of the jet and can be compared against those developed within the framework of the SOM.

3 Results

3.1 Atlantic JJA SOM space

The results of the SOM training are summarized in figure 5 in a grid that represents its topology. Each panel is a wind speed composite of all timesteps belonging to the corresponding cluster. The population of each cluster is shown in Figure 6a). The jet finding and categorization algorithm is applied to these composites, and the results are overlaid with purple and pink lines for the extratropical and STJs, respectively. Since composites have lower wind speeds than instantaneous data, the point-wise wind speed threshold is lowered to $20\,\mathrm{m.s^{-1}}$ and the jet-wise integrated wind speed threshold to $3 \times 10^8\,\mathrm{m^2.s^{-1}}$. Long jets that exhibit a EDJ region and a STJ region (see section 2.3.1) are split into two automatically, on clusters 1 and 7, so that we can later on derive jet properties directly from the SOM composites, in Appendix C.

We first assess a few regions of interest in the SOM from a qualitative study of the composites. Clusters where both jets are present and overlap zonally (double jets) are located on the right side of the grid and the bottom row. A subsection of this

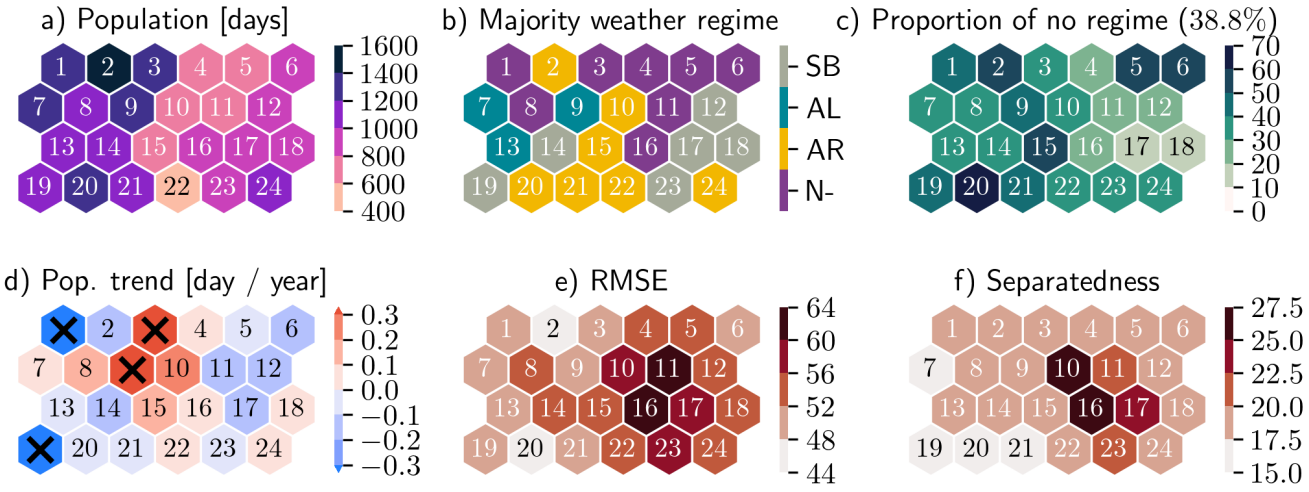

Figure 6. Climatological SOM cluster-wise properties. a) Population, in number of days in JJA 1959 to 2022. b) Weather regime with maximum relative occurence frequency to each SOM cluster, excluding "no regime" the shorthands correspond to NAO- (N-), Atlantic Ridge (AR), Atlantic Low (AL) and Scandinavian Blocking (SB). c) Proportion of timesteps withing each SOM cluster not associated with any weather regime, as in Grams et al. (2017), in percents. d) Trends (1959 - 2022) in population in days per JJA. Significant trends at the 95th percentile are marked with black crosses. e) Root mean square error of each cluster. f) Separatedness of each cluster, as defined in the main text.

high-overlap region of the grid on the center-right columns, clusters 16, 17, 22 and 23, have the subtropical jet over the Sahara while for most the other clusters with double jets, the STJ is further north above the Mediterranean. The EDJ is especially wavy in clusters 2, 6, 9, 12, 13, 14, 17, 18 and 24. Clusters 11 and 16 contain more noisy and small scale jet features than the rest of the SOM. In the composites of cluster 2, the region of high wind speed at the eastern edge that could be interpreted as a STJ is too weak and short in the domain to be captured by the jet detection algorithm.

Figure 6 shows six SOM cluster-wise properties using a hexagonal grid representing the SOM. The first property (panel a) is the cluster population. There is up to a factor > 3 between the least and the most visited cluster, and the left side of the SOM, featuring shorter and weaker STJs, is a lot more represented than the right side. The least populated cluster, 22, corresponds to a south-shifted STJ with a wavy EDJ, while the most populated cluster, 2, features a strong, elongated and wavy EDJ and doesn't feature a visible STJ.

The clusters are related to the summer Euro-Atlantic weather regimes (figure 6b and c) to simplify their interpretation and compare both approaches. This is done by calculating the weather regime occurence probabilities conditional on each SOM cluster occupancy. The most represented weather regime in each SOM cluster, excluding "no regime", is shown on panel b, while the proportion of timesteps during which a SOM cluster is occupied but no regime occurs is presented on panel c. Clusters 18, 12, 17 and 14 are associated with the Scandinavian Blocking regime, and the corresponding relative occurence frequencies are the highest in all the cluster-regime pairs (not shown). This is probably due to the distinctive footprint blocking

has on the jet, a large poleward shift of the EDJ above Europe. Interestingly, cluster 13, which has a very similar jet structure, is not as strongly linked to this regime but instead to the Atlantic Low regime, along with clusters 7 and 9. The NAO- regime is expectedly associated with SOM clusters with a very zonal EDJ, (1, 3, 4, 8 and 11) although the conditional probabilities remain low. The Atlantic Ridge is not strongly associated to any SOM cluster in particular, and the "no regime" appears frequently in most SOM clusters, up to 70% of the time.

In panel d, inter-annual population trends are shown for all clusters. The most negative trend in population, cluster 1, corresponds to a zonal EDJ and a short, north-shifted STJ and is strongly associated to NAO- (panel b). The second most negative trend, cluster 19, features a zonal EDJ and weak, north-shifted and elongated STJ and is not strongly associated to any weather regime. The strongest positive trends, (clusters 3 and 9), correspond to strong EDJ situations, one zonal (3) and one wavy (9), as well as weak and short STJs, without strong association to any weather regime.

We also provide two quality metrics for each SOM cluster: the associated RMSE (figure 6e), where a high value represents a cluster whose weight matrix is a poor representative of many of its members, and the separatedness (figure 6f), where a low value represents a cluster whose weight matrix is very similar to that of its neighbors. We see hotspots in both RMSE and separatedness for clusters 10, 11, 16 and 23. These clusters contain more diverse synoptic situations (high RMSE) than the other clusters, and that are different in their mean to the rest of the clusters, especially those close to them on the grid.

Next, we show the typical JJA pathway through the SOM in figure 7. This figure shows weekly-binned cluster populations for all weeks of JJA and averaged over all JJAs 1959 to 2022. It shows that a small subset of clusters in the center-right columns of the SOM represents most of the circulation during the first week of June, while clusters on other columns are much more likely to be visited in July and August, indicating a marked transition of the circulation patterns during June, in the mean over all years. The shift from the center right columns to the center left and edge columns of the SOM grid at the end of June corresponds to a reduction in double jet occurence and an increase in mean STJ latitude, particularly in July and August.

The first week of June, which is climatologically different from the rest of JJA, has its variablity almost entirely constrained to a few clusters, 10, 11, 16, 17 and 23 (7). The RMSE on these clusters is higher than for the rest of the SOM (figure 6e). The clusters previously identified as early June clusters are almost never populated again past the first of July. The clusters on the upper left corner (1, 2, 3, 7, 8 and 9) are the most populated in late July and early August.

3.2 Jet stream properties

Using the detected and categorized jets, we study the properties of each jet category separately. We have defined numerous jet properties and many of them are correlated with one another, so only a selection of six are shown in the main text, while results for a larger selection are presented in Appendix B.

The six properties chosen have all seen keen interest in the literature. The average latitude can be compared to the JLI (Woollings et al., 2010) while the max. speed can be compared to the JSI or to the 99^{th} percentile of wind speed (Shaw and Miyawaki, 2024). The (inverse of the) jet's COM speed can be viewed as a proxy for persistence. The waviness, as defined by Di Capua and Coumou (2016), and hereafter named DC16 waviness, is a simple metric to quantify the departure from zonality of the detected jets. The width of the jet is emerging as another feature of interest in recent literature (Peings et al., 2018) and

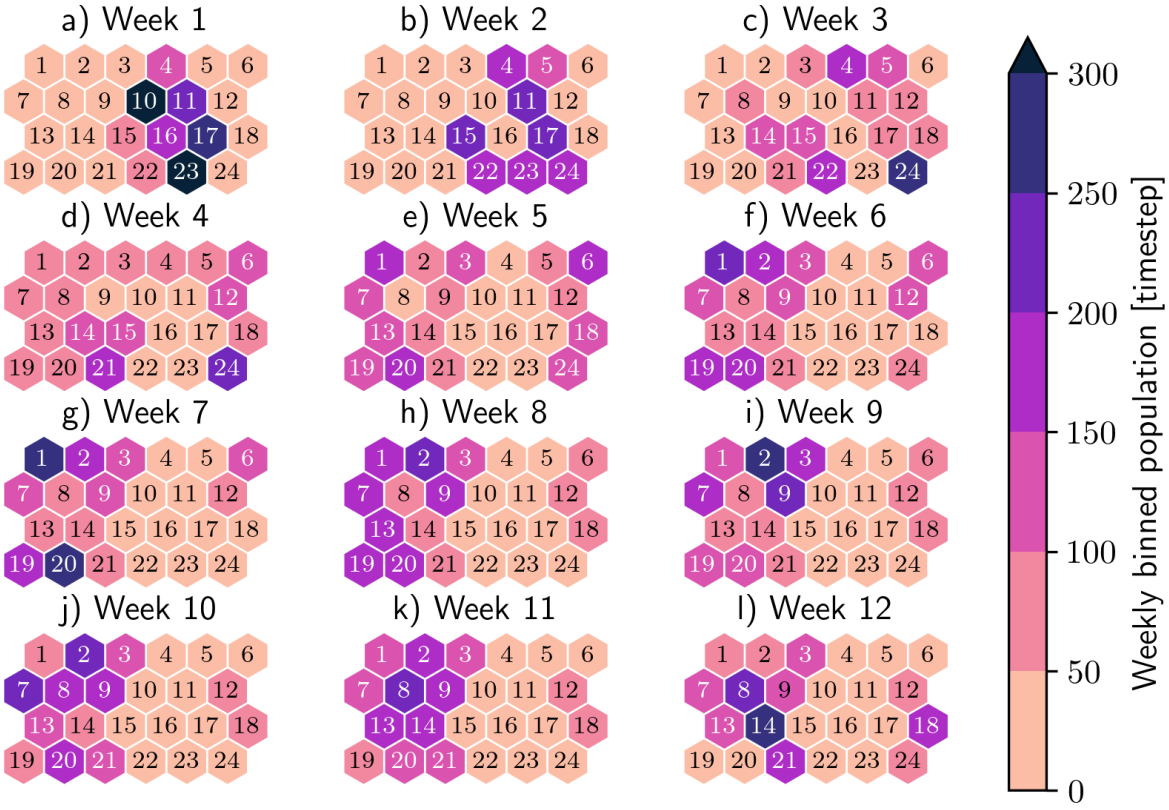

Figure 7. Weekly JJA pathway, the weekly-binned cluster population for all weeks of JJA and averaged over all JJAs. Week 1 corresponds to the first week of June and week 12 to the previous to last week of August.

is here computed using natural coordinates. Finally, we determine, at each longitude, if both jets are present and average this overlap boolean quantity over the European sector ($\lambda > 10$ °W). The mean latitude, max. speed and width distributions have low skew, while the COM speed, waviness and double jet index's distributions are very skewed with tall peaks at low values and long tails.

The seasonal variability of this selection of jet properties is presented in figure 8. Several interesting features can be observed in this figure. First, the month of June is once more highlighted as a transition month that is different from the rest of JJA. More precisely, the speed of both jets and the waviness of the STJ reduce in the months leading up to June (figure 8b and d). Then, during June, both jets move poleward, with a much more pronounced shift for the STJ (figure 8a).

The seasonal variability in latitude and speed of the EDJ are very comparable to the Jet Latitude Index and Jet Speed Index seasonal variabilities (Woollings et al., 2014) and the storm track seasonal variabilities (Hoskins and Hodges, 2019) for the equivalent EDJ properties (respectively average latitude and max. speed). The amplitude and width of the JJA peak in STJ

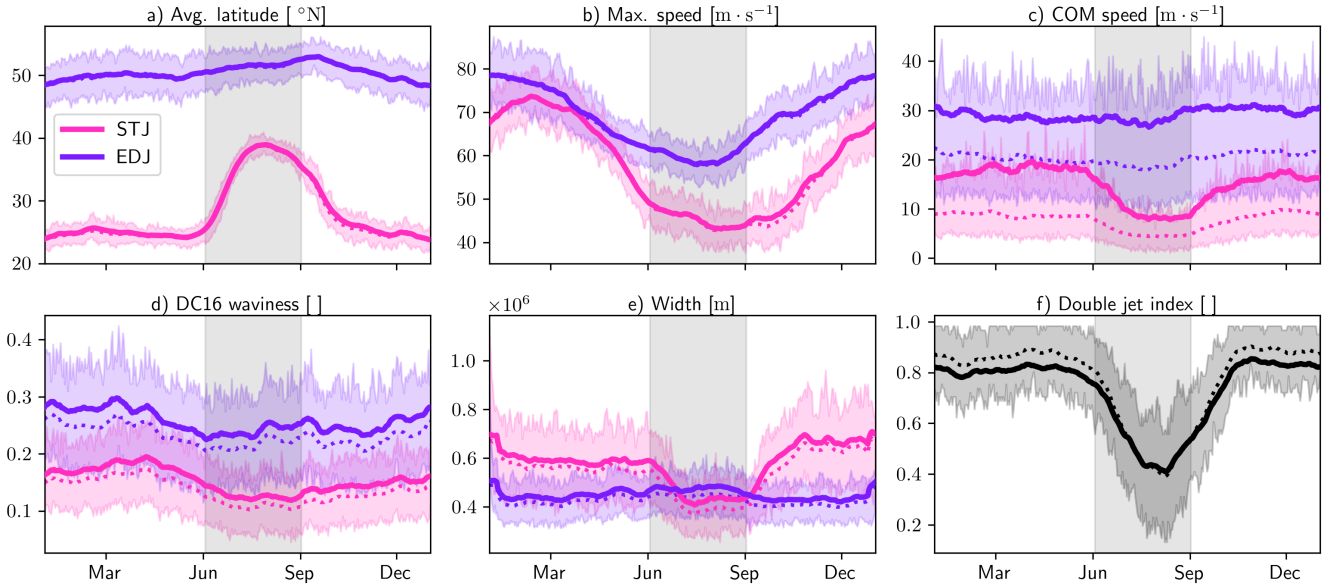

Figure 8. Euro-Atlantic jet properties seasonal variability. The results are split by jet category and always colored in the same way: pink for the STJ and purple for the EDJ. The double jet index is colored in shades of gray. A 15-day-window averaging is applied to the day-of-year mean (thick line) as well as the day-of-year median (thin dotted line) but not to the inter-quartile range (shading). The marker label for each month corresponds to the first day of this month. The grey rectangle in the middle of each panel represents JJA.

latitude can be compared with Maher et al. (2020). Seasonally, the STJ follows the expansion and weakening of the Hadley cell in the northern hemisphere summer (Dima and Wallace, 2003; Davis and Rosenlof, 2012).

The speed of the COM, the DC16 waviness and the width do not show strong seasonal variabilities in contrast (figure 8c, d and e), with signals staying well below the interannual variability, with the exception of the STJ's waviness which shows a peak in spring, and a slight dip in EDJ width in summer compared to winter. The jets are much closer together in JJA than the rest of the year, but overlap less often, mainly due to the subtropical jet occuring less often in JJA (see fig 4).

An important question is how these properties have evolved under the past climate change. Figure 9 shows the inter-annual JJA trends for the selected six properties. Statistical significance is tested using block bootstrapping, with 10'000 bootstrapped time series created with a block size of four years.

Trends in JJA are yet to emerge out of the inter-annual variability, as only three of the eleven trends shown in figure 9 are significant, a negative trend in the max. wind speed of the STJ and a positive trend in the waviness of both jets with the DC16 definition. The STJ max. wind speed trend is consistent with the findings of D'Andrea et al. (2024), who report a significant decrease in zonal wind between -0.1 and -0.5 m/s per decade an the area corresponding to the location of the STJ in JJA (see figure 5). The trends in waviness, while large in this figure, are dependent on the definition, as we showcase in Appendix B. An increase in waviness in this region is consistent with, e.g. Francis and Vavrus (2015) and Cattiaux et al. (2016). It is also consistent with a positive trend in occurence frequencies for SOM clusters featuring wavy or tilted (3, 9) and negative trends

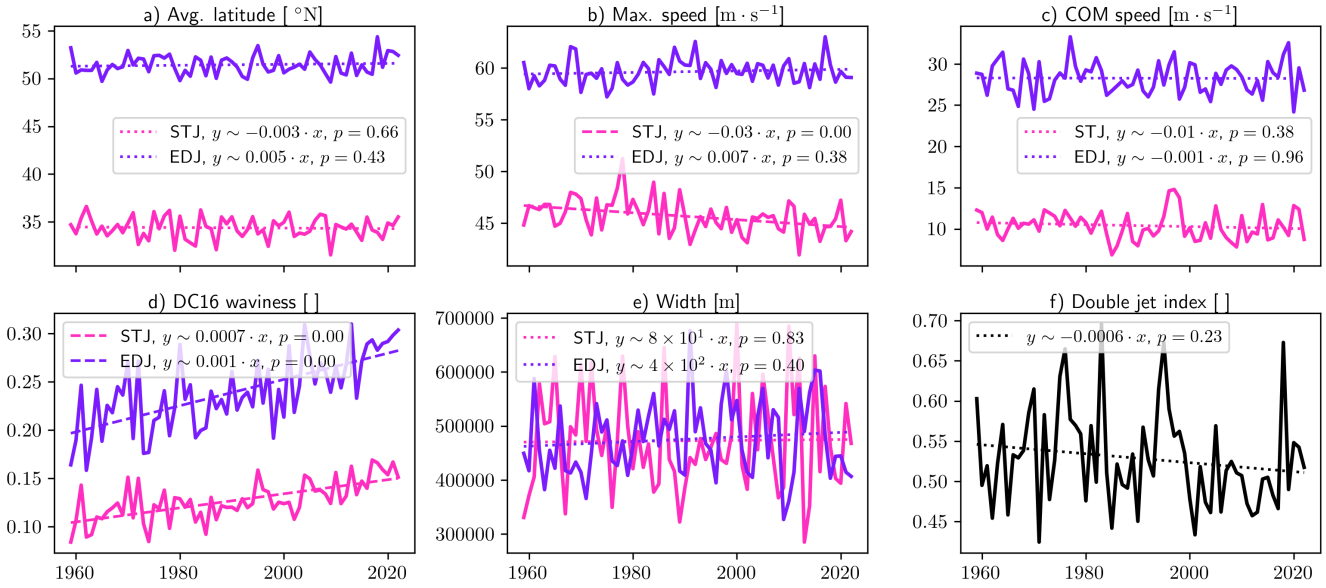

Figure 9. Euro-Atlantic jet properties JJA means and inter-annual trends, split by jet category. Linear trends represented by dashed lines are significant at the 95$^{\text{th}}$ percentile, while the dotted lines are not.

in clusters presenting more zonal jets (1 and 19). It is worth mentioning that, with our definition, there is only a non-significant negative trend in double jet index in this domain.

Trends of these six jet properties can be viewed at a finer temporal scale, for each day of the year on figure 10. The significance is once more established using block bootstrapping with the same settings as for figure 9, and it is assessed prior to the 60-day rolling-window smoothing.

The EDJ exhibits a poleward shift accross most seasons, consistent with the arguments of Held (1993) (figure 10a). The STJ shows an equatorward trend in spring and a poleward trend in autumn (figure 10a). The EDJ maximum wind speed increases consistently accross the whole year, with the strongest of intensification in February, March, May and June (figure 10b). This result can be linked to results in past data (Woollings et al., 2018a; Harvey et al., 2023), and in future simulations Shaw and Miyawaki (2024). The STJ has opposite trends in its max. speed between JJA, where the trend is negative, and September to December where the trend is positive (figure 10b). No strong trends appear in our results for the COM speed, except a negative trend in COM speed in July and August for the EDJ and in Sepember and October for the STJ (figure 10c). DC16 waviness increases significantly, for both jets and consistently over the whole year, with a stronger increase between January and June (figure 10d), which is mostly consistent with , e.g. Cattiaux et al. (2016) and Di Capua and Coumou (2016), albeit in different regions. The width does not show strong trends except a negative trend in April and May for the STJ (figure 10e). Finally, the double jet index increases significantly in March, April and May and decreases significantly in July and August (figure 10f), although the trends in JJA averages were not significant (figure 9).

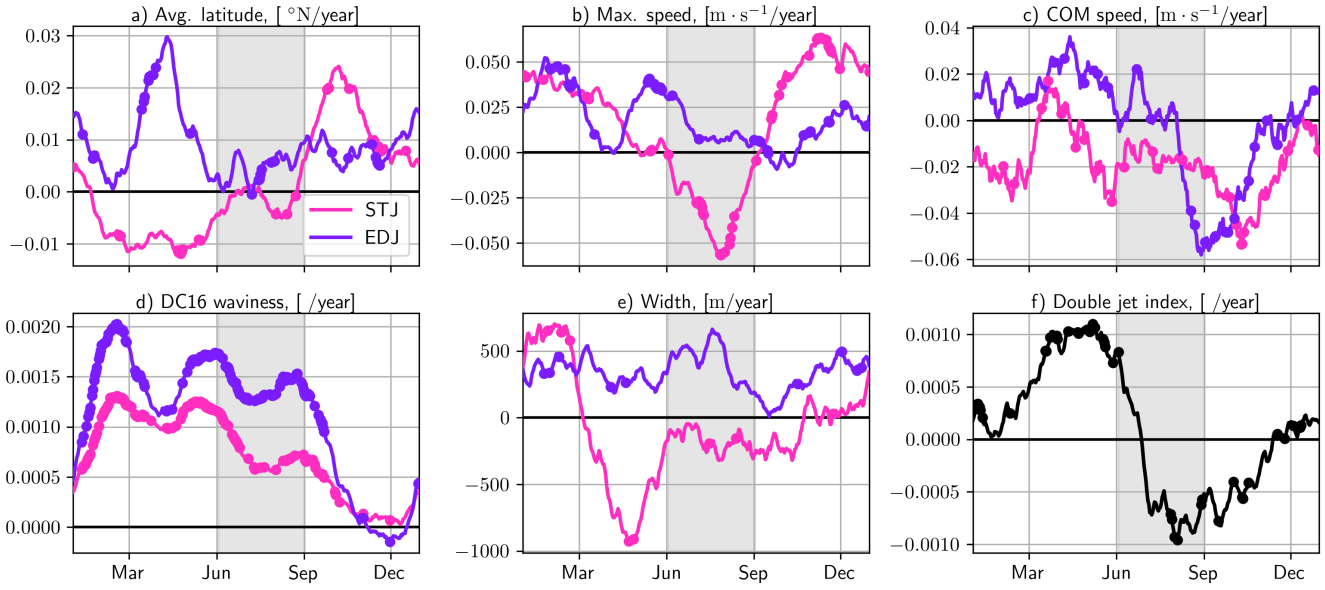

Figure 10. Euro-Atlantic jet properties inter-annual trends, computed independently for each day of the year, and the result smoothed by a 60-day rolling window. Trends significant at the 95th percentile are marked with a thick dot. Significance is assessed prior to smoothing.

3.3 Jet properties on the SOM

In this section, we make use of the detected jets and their properties to assess the capabilities of the SOM to capture jet stream variability as opposed to random noise. First, we composite jet core detection probability, separated by jet category, and overlay the jet cores found in the SOM wind speed composites, i.e. figure 5. The results, visible in figure 11, show a clear agreement on the position of the detected jet cores as well as on their categorization.

As a way to compare and validate the results of both methods, a selection of jet properties are projected onto the SOM clusters, shown in figure 12.

The latitude of the EDJ is, as on the composites, higher on the extremal columns than in the central columns of the SOM (panel a), and the clusters with highest mean EDJ latitude also correspond to clusters with high relative occurence of the Scandinavian Blocking weather regime (see figure 6b). The maximum speed of the EDJ is highest on clusters 10, 14 and 23. These three clusters have the highest population during the first (10 and 23) or the last (14) week of JJA (see figure 7), when the EDJ has the highest max. speed in JJA (see figure 8). Similarly, the EDJ max. speed is lowest in clusters populated in the middle of JJA (clusters 1, 7, 12, 19, 20). The EDJ waviness is highest on most cluters associated to the Scandinavian blocking or Atlantic Low regimes, and lowest for clusters associated to the NAO- or Atlantic Ridge regimes, with the notable exception of cluster 8, weakly associated with NAO- but very wavy (see figure 6b, relative occurence not shown).

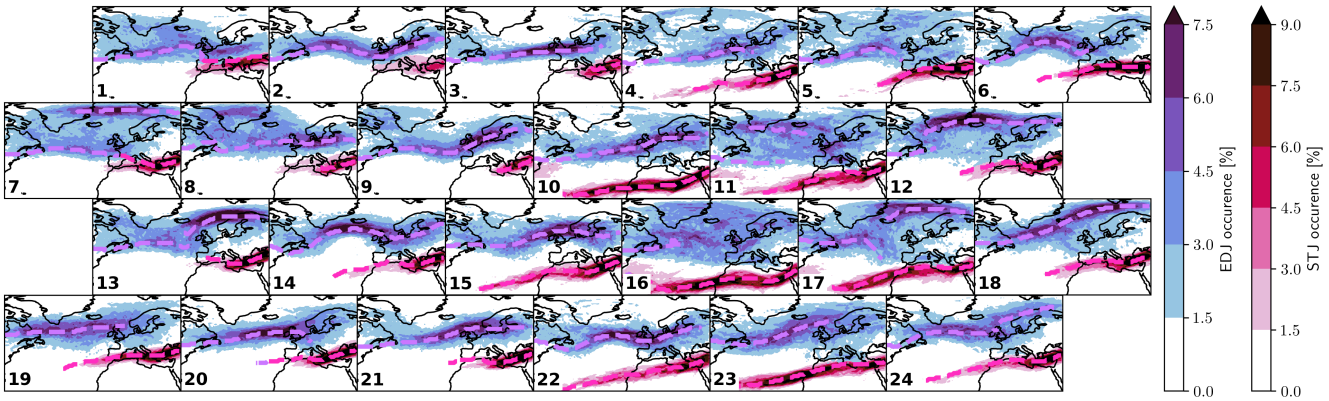

Figure 11. Jet core detection probability composites (blue shading for EDJ, pink shading for STJ), and jet cores found on wind speed composites, figure 5, as colored lines (purple for EDJ, pink for STJ).

The double jet index, as well as the max. speed, mean latitude and width of the subtropical jet all follow the very clear seasonal signals presented in the previous section (figure 8) when matched with the weekly cluster populations (figure 7). The observations are also very consistent with what can be seen on the jet core probability composites (figure 11).

The observations made, qualitatively, on the wind speed composites (figure 5), can all be matched with the jets' mean properties on the clusters (figure 12). This result is not entirely trivial. It means that, for most clusters, the jets found in the cluster mean wind speed composites have properties corresponding to the mean of the properties of the jets found in each individual timestep belonging to that cluster. In other words, the wind composites and the jets found therein are representative of the wind speed snapshots, as well as their jets, belonging to each cluster and not merely artifacts of averaging noisy fields. These observations are quantified in Appendix C.

3.4 Jet persistence

We characterize persistence using three metrics extracted from the residence times on each SOM cluster and two metrics for each jet category, the jet lifetime and the speed of the center of mass. To compare all of these metrics, we aggregate their results for each SOM cluster and plot the results in a hexagonal plot as in section 3.3.

Our definition of residence times allow for departures one cluster away from the origin cluster (see section 2.2.3). We first count the number of stays that last more than 4 days on each SOM cluster (figure 13a). The lengths of stays of any length are aggregated as JJA averages (panel b) and 95th percentiles (panel c). The summer averages give an approximation of the state persistence (Tuel and Martius, 2023), i.e., an estimate of how much time the large scale-scale circulation pattern typically needs to move from one state into the next, while the number of long stays and the 95th percentile of residence times capture more episodic persistence, i.e., the most persistent events of each flow configuration.

Clusters 1, 2, 3 and 20 are characterized by a large number of long stays, and a high state and episodic persistence. These clusters all represent a roughly similar synoptic situation of a zonal EDJ extending over the British Isles and with slightly

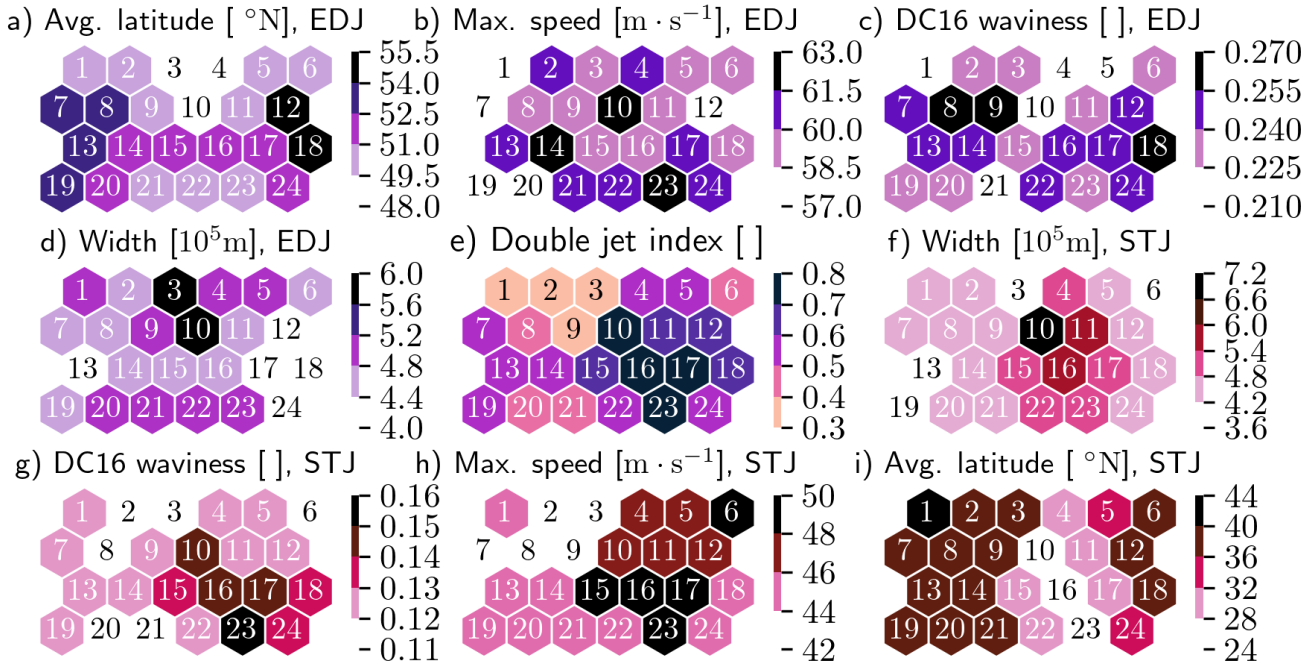

Figure 12. Jet properties, separated by jet category when applicable, projected on the SOM clusters. Shades of purple corresponds to EDJ properties and shades of pink to STJ.

positive tilt, but with minute differences in apparent EDJ waviness and length of the STJ. These are very well-defined clusters (low RMSE) but with the lowest separatedness in the SOM, which confirms our observations on their composites. In the rest of the SOM, the state and episodic persistence seem to be correlated, and the previously highlighted region of clusters representing the first week of June (10, 11, 16, 17 and 23) does not stand out as more or less persistent than the clusters representing the rest of JJA.

Results from the projection of jet-wise persistence metrics onto the SOM show mixed agreement with the SOM persistence metrics, at least in this presentation of temporal aggregates, as well as mixed agreement among each other. High COM speeds of either jet, which indicate low instantaneous persistence, can be associated with either low or high state persistence, and with either low or high jet lifetime, for jets of the same nature or the other. It is worth reminding that, while all of these numbers characterize persistence in some sense, they are very different in nature. Jet lifetime and SOM average residence time are both nonlocal, which means they can only be determined when a jet has weakened below the jet integral threshold or left the domain, and when a stay on a SOM cluster has ended. Additionally, the two jet related metrics only assess the persistence of one jet at a time, which can be very different. This can make these metrics unfit to qualify a timestep or a period concisely.

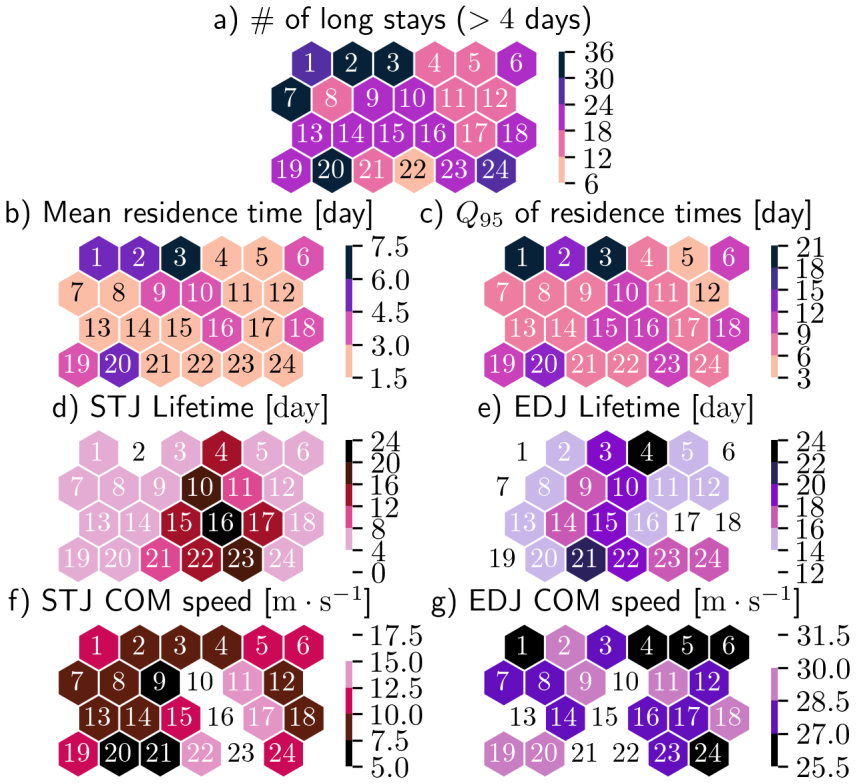

Figure 13. Persistence properties of the SOM clusters. a) Number of long stays on each SOM cluster. b) Mean residence time on each SOM cluster. c) 95$^{\text{th}}$ percentile of residence times on each SOM cluster. The definition of residence time here is loosened to allow a for a stay to be unbroken as long as the jumps are to a cluster similar enough to the starting cluster (below the 10$^{\text{th}}$ percentile of pairwise distances between cluster weight matrices). d-g) Jet persistence properties, separated by jet category when applicable, projected on the SOM. Shades of purple corresponds to EDJ properties and shades of pink to STJ.

4 Discussion and summary

We use two complementary methods, self-organizing-maps (SOM) and jet core detection, to characterize the upper-level tropospheric jets, and apply them to the Euro-Atlantic sector in the less studied northern hemisphere summer season, along with some year-round results. The SOM method specializes in finding dynamical properties of the overall flow, including persistence, while the jet core detection method finds properties of individual jet cores at individual timesteps, and present for each the ERA5 inter-annual trend and intra-seasonal variability. These methods have overlap: for example the SOM shows a clear intra-seasonal variation in cluster population, and some of the jet properties are proxies for persistence. These overlaps allow us to verify the results between methods, increasing our confidence in our results.

The SOM, a clustering method with distance-preserving properties, allows us to study the circulation time series as a sequence of stays on a cluster and jumps between clusters, where the magnitude of the jumps is meaningful. A group of clusters with low population, high mean cluster error, high cluster separatedness, and a south-shifted STJ compared to the other clusters, is shown to be comprised almost entirely of timesteps in the first one or two weeks of June every year. This time of the year is therefore identified as having a very different mean synoptic situation to the rest of JJA, but its relatively low weight in the data compels the training algorithm to only assign a few clusters to it, too few to correctly capture the variability of this period.

The SOM is related to weather regimes using relative occurence frequencies. With strict conditions for regime occurence, a high proportion of JJA days is not assigned to any regime, and only a few SOM clusters can be strongly associated to weather regimes, typically to the Blocking regime which is accompanied by a poleward shift of the EDJ above Europe, easily captured by our wind-based clustering approach.

Long stays on a SOM node is a natural way to evaluate state persistence. The most persistent clusters correspond to long EDJs that extend over the British Isles, and north-shifted, short and weak STJs over the Mediterranean. Aside from those rough similiarities, they present differences in EDJ waviness and maximum speed according to the mean jet properties projected on the SOM. These clusters, which have high occurence probability and persistence, typically do not project well on any weather regime. This is a strong incentive to consider using more clusters than four, irrespective of the clustering method employed, when it is compatible with the research question. In this study, the larger number of clusters has allowed us to describe the majority of JJA timesteps as cluster visits with low projection error, and has all but guaranteed that all the persistent episodes can be extracted as long stays on SOM nodes, with our definition.

A variation of the jet core detection algorithm presented by Spensberger et al. (2017) is used to identify instantaneous jets and extract properties for each of them separately. The jets are classified into the two canonical jet categories (subtropical and eddy-driven jet, respespectively STJ and EDJ), and tracked over time to obtain metrics that offer another view of persistence. Once more, past trends and seasonal signals are extracted.

In JJA, the only significant trends are an increase of the DC16 waviness of both jets and a slowdown of the STJ. The poleward shift of the EDJ projected in, e.g., Held (1993), is not significant in our analyses in JJA, nor is the equatorward trend of the STJ reported by Totz et al. (2018). The absence of a trend in STJ latitude, seemingly at odds with the measured tropical expansion (e.g., Davis and Rosenlof, 2012), is consistent with findings in the recent literature (Davis and Birner, 2017; Maher et al., 2020).

Year-to-year trends, computed independently for every calendar day, vary a lot over the year at subseasonal timescales. The trends in 3-monthly averages that are often presented in literature can therefore sometimes be misleading, as they can average out strong trends of opposite signs. As an example, the double jet index has a strong positive trend before and up to June, and a strong negative trend in July, August and September, so its trend in JJA average is weakly positive. Still, it is useful to continue discussing these trends in seasonal averages, to create points of comparison with the past literature and because they allow us to illustrate the different amounts of interannual variability between jet properties.

Comparing results from the two methods, SOM and properties of the detected jet cores, helps to validate them. The SOM is shown to capture jets and not random noise, because the jet cores detected on the composited wind fields match very well with the probabilities of jet core detection, composited for every cluster. The expert-defined jet properties do succeed in characterising features which dominate the leading patterns in the more statistical SOM approach. Computing properties of the jets at every time step before averaging them based on cluster membership gives very qualitatively similar results to computing jet properties on the jet cores extracted from each cluster wind speed composite, but the match is not perfect. Furthermore, the strong regime shift happening in June, characterized most clearly by a weakening and poleward shift of the STJ, is distinctly picked up by both methods. Trends in waviness can be matched to positive trends in clusters with wavy or tilted jets. As a more subtle point, clusters that represent early June and have the highest mean double jet index within this subset get more frequent, albeit weakly, than the rest of this early June subset, while the opposite is true for the July-August subset of SOM clusters, which matches well with the opposite sign trends in double jet index between early and late northern hemisphere summer. This indicates that both methods are mostly coherent with one another.

The persistence metrics developed around the jet detection method show another facet of persistence to the one expressed by the SOM cluster residence time, and the results of both methods often disagree. This is partly explained by their many differences in nature. Only the jets' COM speeds can be assessed locally in time, and the jet related metrics only refer to persistence of a single object at a time, different from the state or episodic persistence quantified by SOM residence times.

The jet detection algorithm is directly applicable to global data, as are the jet properties computation and the jet tracking. A global jet categorization would, however, have to use an adapted set of jet properties to distinguish the EDJ from the STJ, as longitude and latitude are only good discriminants in the Atlantic basin. A different set of jet properties might have to be used for each season or even each month, as the seasonal signals suggest. The SOM, like all clustering metrics, is not well suited for a global application and works best when restricted to a single basin. The steep increase in dimensionality and variability that accompanies an expansion to a larger region, combined with the same proportionally small number of timesteps, creates a much more ill-defined clustering problem. Since both methods are relatively cheap computationally, they can be applied to large ensembles and higher-resolution model data to evaluate future trends and shifts in seasonal signal or persistence and predictability properties.

In future work, we will use these diagnostic tools to study the circulation before and during extreme weather events in Europe. Potential applications currently explored include assessing atmospheric persistence and predictability properties in the days leading up heatwaves, finding SOM clusters most likely to see the onset of a damaging hail storm, and discovering which jet properties can be used as good predictors for extreme surface winds in a statistical model.

The previous paragraph pertains to the jet stream as a potential driver of weather predictability, even if the causality can go in both directions. Another use for the methods is the investigation of the drivers of jet stream variability, for example, large-scale teleconnections like ENSO or local mechanisms like diabatic heating, as has been studied recently by Auestad et al. (2024). Another avenue is the exploration of the jets' tight relationship to Rossby waves, for example by assessing the ability of the detected jets to carry and guide Rossby waves (Martius et al., 2010; Wirth, 2020; Wirth and Polster, 2021; Bukenberger et al., 2023; White, 2024). Similarly, it is now easier to examine their relationship to Rossby wave breaking, for instance as triggers

of large jumps in SOM clusters (Michel and Rivière, 2011), or as drivers for abrupt changes in jet strength, latitude, or center of mass speed (Martius and Rivière, 2016). Adapting the jet width method to instead find wave breaking events around the jet core is showing promising early results.

Code and data availability. The ERA5 reanalysis data are publicly available at https://cds.climate.copernicus.eu. The SOM training and visualization code (hexagonal plots) was adapted from https://github.com/fcomitani/simpsom, and the rest of the code can be found at https://github.com/hbanderier/jet_stream.

Appendix A: Further exploration in jet categorization

On figure A1, we explore the effects of changing the categorization method on the seasonal variabilities of the categorized jet properties. First, on the first three rows of the figure, we vary the cutoff between STJ and EDJ. The effects on the mean position (in latitude and pressure level) is barely distinguishable, but the effects on the number of jets of each category per timestep can be markedly altered by this choice, especially for the STJ when changing the cutoff from 0.1 to 0.5.

Then, we allow jets whose categorization score is between 0.1 and 0.9 to be assigned to the hybrid category. The aggregated properties for the three jets can be seen on the fourth row of figure A1. As many jets belong to the hybrid category as to the STJ in winter, while in JJA there are more hybrid jets than STJ, according to this cutoff. However, this hybrid jet has an almost identical seasonal cycle to that of the STJ, in its spatial distribution but also in its other properties (not shown). We therefore decided against introducing this third category in the paper, since it seems to behave like a STJ. This is also why we choose a cutoff of 0.9 in the main text. This way the STJ corresponds to well defined STJs as well as hybrid jets which we identify as worse-defined STJs.

We would interpret these findings as follows. In JJA, the subtropical jet is shifted north with the Hadley cell and interacts with extratropical eddies more, making it lose more momentum (Martius, 2014) and potentially making it more baroclinic. This makes the distinction more fuzzy, so there are more jets that don't fall cleanly on either Gaussian, i.e. more jets with a score very different from either 0 or 1. These jets still seem to behave more like STJs than EDJs, potentially because most of their momentum still comes from the (sub) tropics and is conserved.

For comparison with our earlier categorization method that used only spatial information (longitude, latitude and pressure level of the jet point), we perform the categorization one last time with this choice of discriminant variables. The results can be seen on the fifth and last row of A1, and shows again similar results. This previous method worked well in the North Atlantic basin but was not based on physical bases and did not generalize well to other basins. Both of those concerns are solved with the new method, that can be applied to hemisphere-spanning jets without modification.

Appendix B: Extended jet properties

In the main text, we have highlighted how many jet properties undergo a transition around the month of June, setting this month apart from the rest of JJA in terms of absolute values of these jet properties.

In order to give a more complete overview of the jet properties, we show the seasonal cycle of the complete set on Figure B1.

Comparing the jet core's mean and max speeds shows little difference between the two in their seasonal cycles. The max speed trends are expectedly stronger but they also seem statistically more robust than mean core speed trends. The waviness metrics all show a different seasonal cycle, and even disagree even on which jet category is wavier than the other. Apart from the differences in the original metrics, this discrepancy can also come from how they were adapted to function on jets, and more specifically the normalization factor used in several waviness metrics ($1/\Delta\lambda$) that favorises high values for the STJ which is typically much shorter in this domain. Another issue is that most of these metrics, from their definition, fail to distinguish

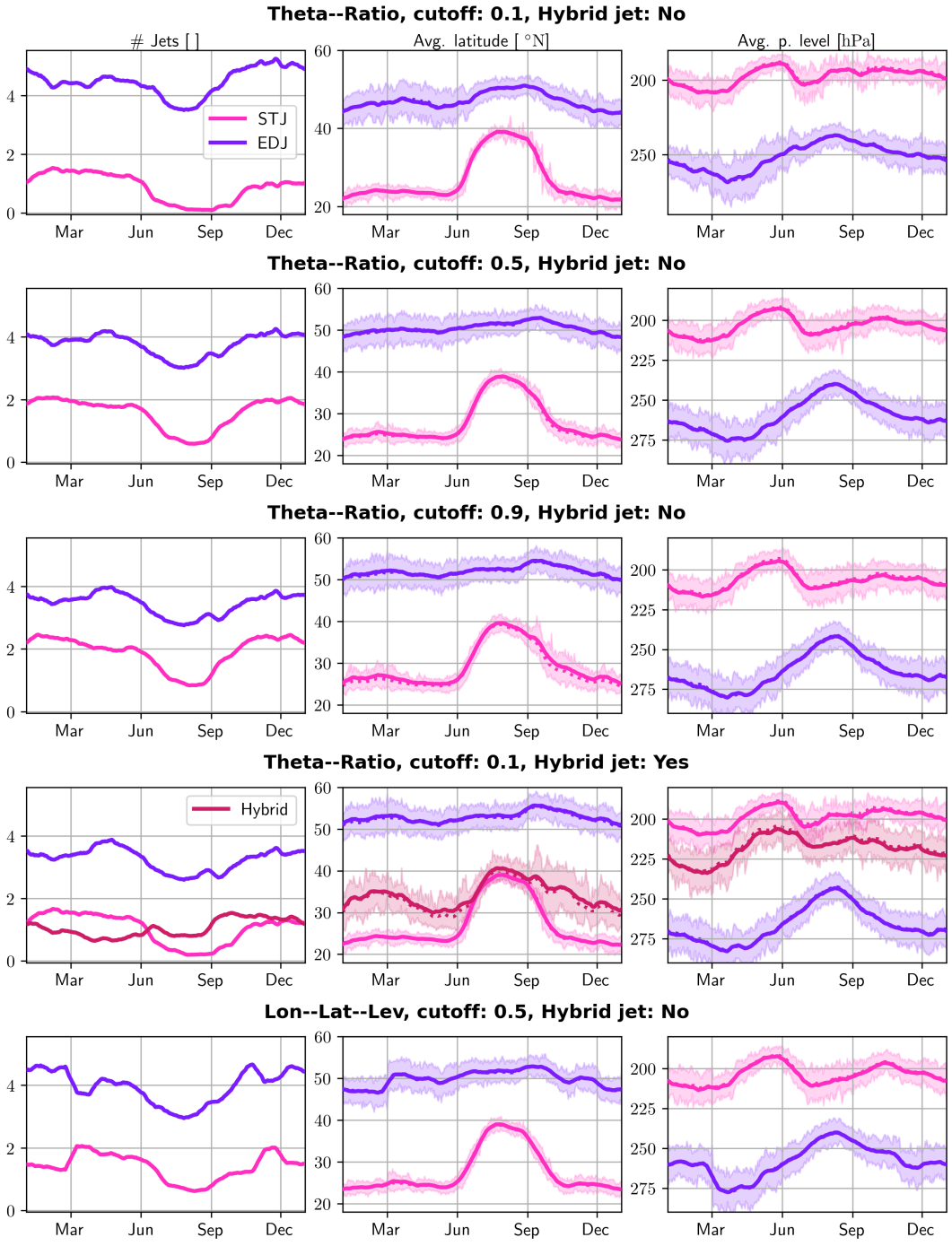

Figure A1. Seasonal variabilities of categorized jet properties with variations in the categorization method.

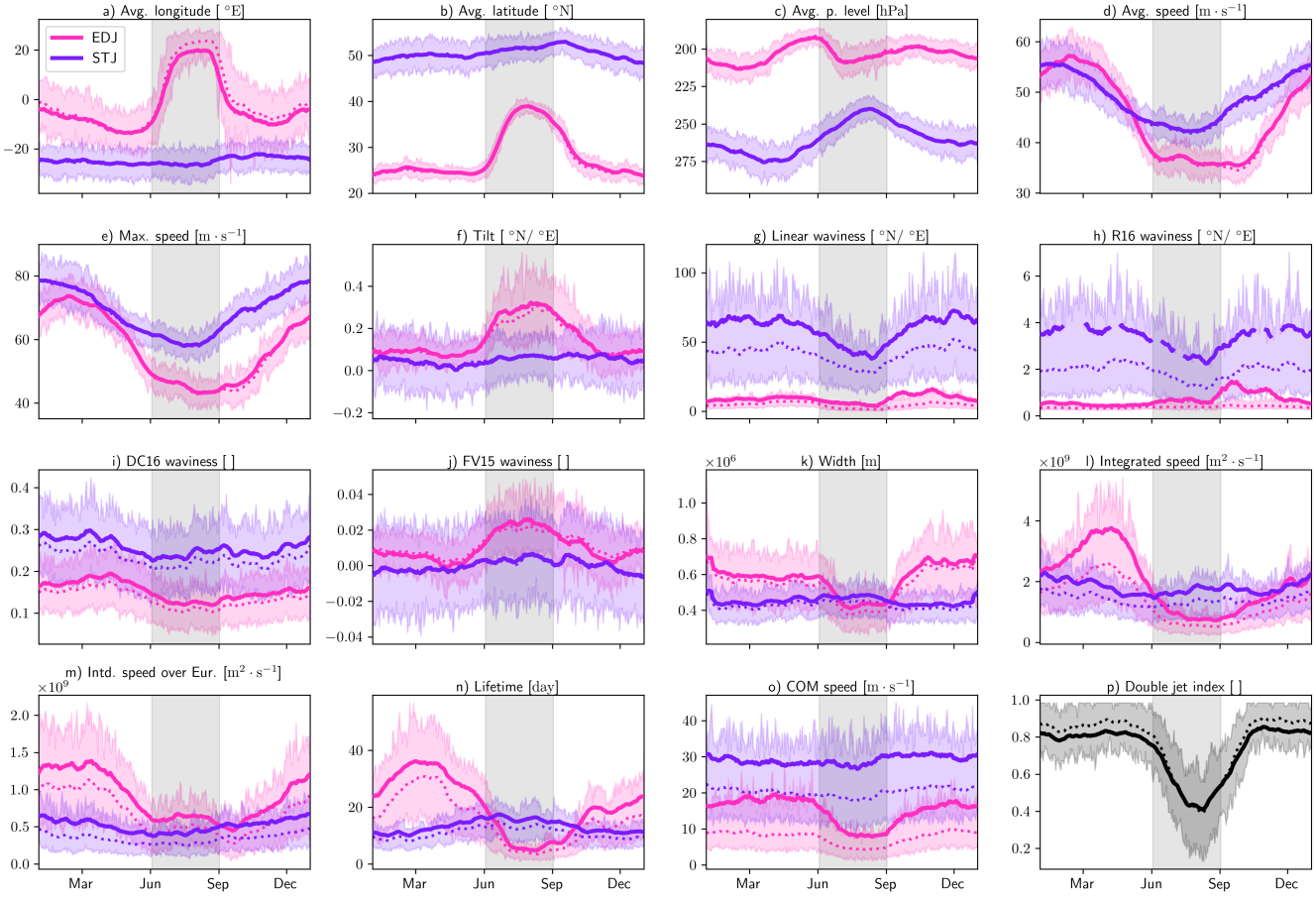

Figure B1. Reproduction of main text's figure 8 with a larger selection of jet properties.

small synoptic scale waviness and tilt. Only our linear waviness is designed to fully separate the two, but proposing another waviness metric is not our goal with this study. FV15 waviness is very close to our definition of tilt, and the seasonal signals of these two metrics are very similar. R16 waviness and linear waviness show an almost identical seasonal cycle too, despite the fact that, from their definitions, one could predict a very different behaviour. Following from our previous comments, it is not surprising that all of the waviness metrics show vastly different trends throughout the year (figure B2).

Appendix C: Properties of the jets detected on SOM composites

In this Appendix, we validate observations made in the main text about the capacity of SOMs to correctly capture the jet properties. We do so by measuring the properties of the jets detected in the wind field composites of figure 5. The results, shown on figure C1, point towards an overall agreement with some caveats. First, the STJ is not detected in the composite for cluster 2, even though it is present in some timesteps belonging to this cluster. Wind speed composites also have lower

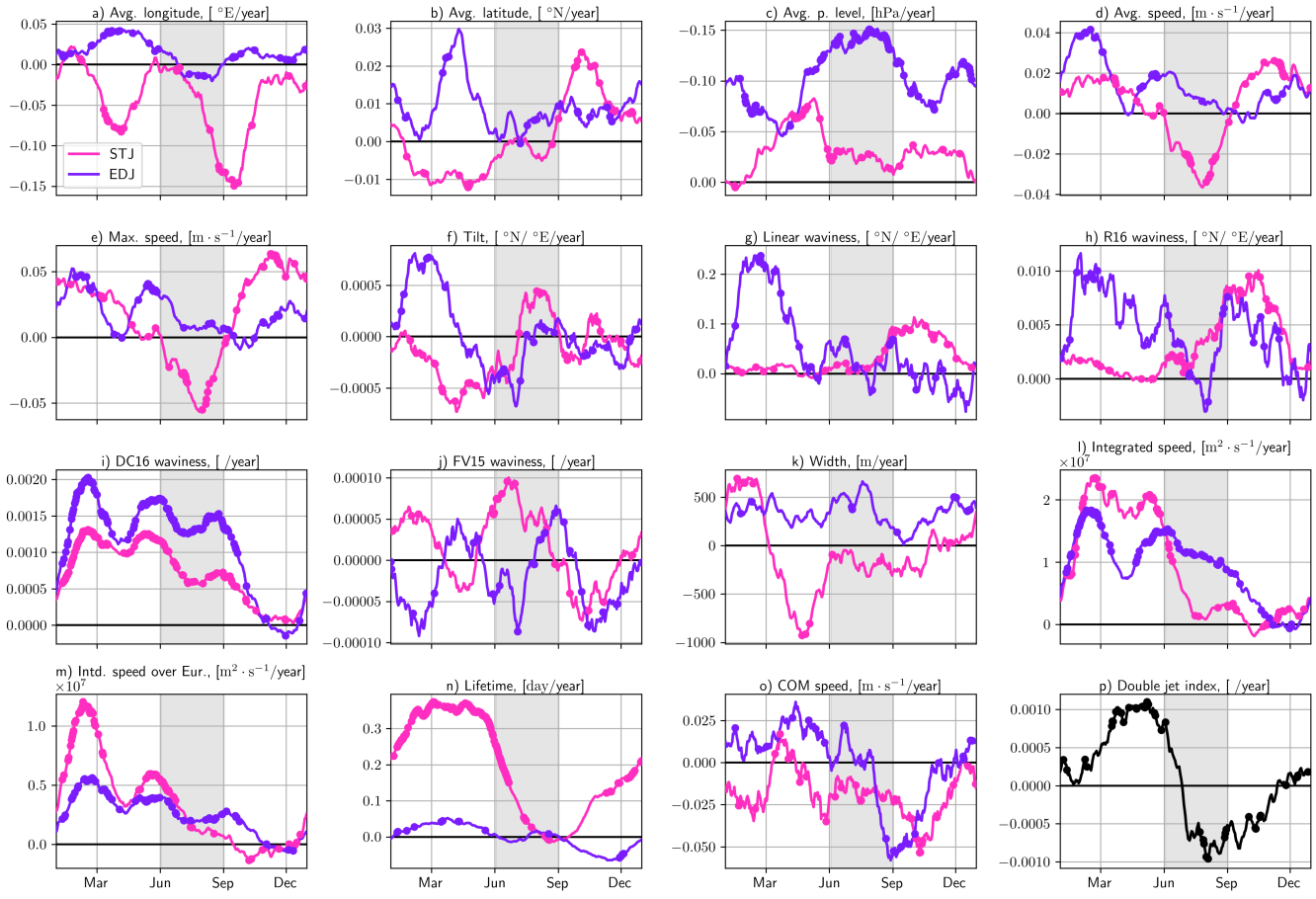

Figure B2. 1959-2022 Day of year inter annual trends, smoothed using 60-day rolling window averaging. Colored points indicate a significant trend at the 95th percentile.

wind speeds than instantaneous fields overall, so the maximum speeds of both jet categories are reduced by about $10\,\mathrm{m.s^{-1}}$. If the absolute values cannot always be meaningfully compared between figures 12 and C1, the distribution of lower and higher values on the SOM can, and in this view there is a large agreement.

Appendix D: Overview of previously tried methods for jet core extraction.

During the development of the jet core extraction algorithm, several different avenues were explored to improve its robustness or the execution speed and later abandoned in favor of the final version of the algorithm presented in the main text. We believe it is valuable to present negative results, both because these methods could be improved and used again in other relate applications, and simply for future researchers in this field not to repeat methods that were explored but ultimately failed at improving the algorithm.

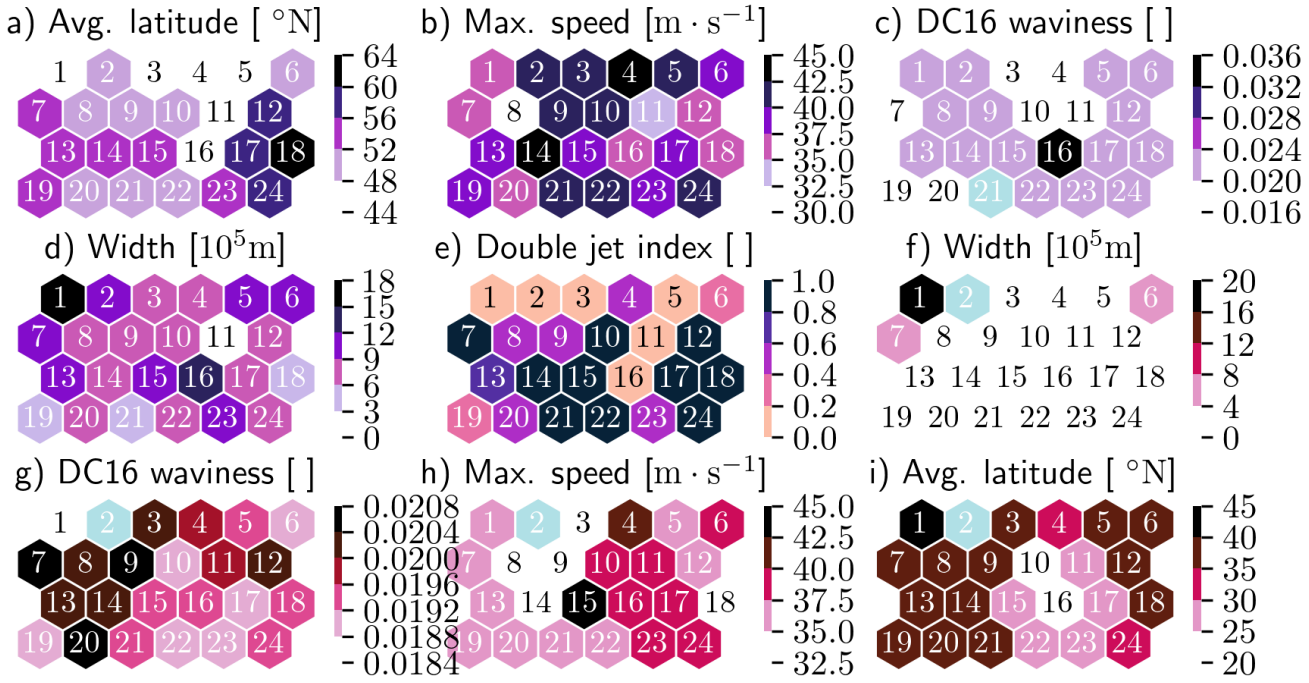

Figure C1. Jet properties, separated by jet category when applicable, computed from the jets detected on the SOM cluster centers. Shades of purple corresponds to EDJ properties and shades of pink to STJ.

The first version algorithm was an adaptation of the Koch et al. (2006) algorithm, also used in Pena-Ortiz et al. (2013). This algorithm uses a peak finding algorithm on each latitude band, before connecting the points longitudinally based on a distance criterion. The peak finding algorithm requires several thresholds, and their tuning is challenging without an objective quality metric to grade the performance of the algorithm. More fundamental problems appear with forked jets, seen in SOM cluster 17 for instance.

The second version divides the task in two. First, potential jet regions are found using a relatively low wind speed threshold, that can be made seasonally varying or even a quantile threshold to work well in all seasons. The regions are separated from each other using spatial agglomerative clustering. The second step of the algorithm is heavily inspired by Molnos et al. (2017). Each potential jet region is turned into a graph, with each gridpoint a node and edges connecting all of the nodes. The edges are assigned a weight based on the wind speed of the nodes/grid points it connects, and on its alignment with the directional wind field (similar to the current algorithm). From potential jets, the jet cores are found using a weighted shortest path algorithm.

The difficulty of this second method comes from jet regions connecting to each other if they are too close, and the problem of determining start and end points of jet cores within the jet, with potentially several starts and ends within each potential jet region because of the first problem. Several avenues were explored to mitigate the first problem, which in turn made the second problem easier to solve. Most notably, the use of computed vision techniques like thinning, skeletonization and Sato

filtering (Sato et al., 1998). This latter technique is used in medical imaging to highlight vessel like structures in black-and-white images like blood vessels in biological tissue, and seems very promising to help in jet detection. However, it also requires careful setting of its parameters, most crucially its filtering scales which loosely correspond to the expected width of the jet in pixels. Solving these problems made the algorithm grow in complexity and computing requirements for little added benefits. This approach as well as other related ones were finally abandoned in favor of the simpler, more robust one presented in the main text.

Author contributions. OM and TW outlined the study. HB developed the code and performed the study under the supervision of AT, OM and TW. HB wrote the manuscript with contributions and reviews from all co-authors.

Competing interests. At least one of the (co-)authors is a member of the editorial board of Weather and Climate Dynamics. The authors have no other competing interests to declare.

Acknowledgements. This work was funded by the Swiss National Science Foundation as part of the project "PERSIST-EUROPE" under grant number 200020_207384.

References

Athanasiadis, P. J., Wallace, J. M., and Wettstein, J. J.: Patterns of Wintertime Jet Stream Variability and Their Relation to the Storm Tracks, https://doi.org/10.1175/2009JAS3270.1, 2010.

Auestad, H., Spensberger, C., Marcheggiani, A., Ceppi, P., Spengler, T., and Woollings, T.: Spatio-Temporal Averaging of Jets Obscures the Reinforcement of Baroclinicity by Latent Heating, Weather and Climate Dynamics, 5, 1269–1286, https://doi.org/10.5194/wcd-5-1269-2024, 2024.

Barnes, E. A. and Hartmann, D. L.: Rossby Wave Scales, Propagation, and the Variability of Eddy-Driven Jets, Journal of the Atmospheric Sciences, 68, 2893–2908, https://doi.org/10.1175/JAS-D-11-039.1, 2011.

Barnes, E. A. and Polvani, L.: Response of the Midlatitude Jets, and of Their Variability, to Increased Greenhouse Gases in the CMIP5 Models, Journal of Climate, 26, 7117–7135, https://doi.org/10.1175/JCLI-D-12-00536.1, 2013.

Barriopedro, D., Ayarzagüena, B., García-Burgos, M., and García-Herrera, R.: A Multi-Parametric Perspective of the North Atlantic Eddy-Driven Jet, Climate Dynamics, https://doi.org/10.1007/s00382-022-06574-w, 2022.

Berry, G., Thorncroft, C., and Hewson, T.: African Easterly Waves during 2004—Analysis Using Objective Techniques, Monthly Weather Review, 135, 1251–1267, https://doi.org/10.1175/MWR3343.1, 2007.

Blackport, R. and Fyfe: Climate Models Fail to Capture Strengthening Wintertime North Atlantic Jet and Impacts on Europe, https://doi.org/10.1126/sciadv.abn3112, 2022.

Blackport, R. and Screen, J. A.: Weakened Evidence for Mid-Latitude Impacts of Arctic Warming, Nature Climate Change, 10, 1065–1066, https://doi.org/10.1038/s41558-020-00954-y, 2020.

Bukenberger, M., Rüdisühli, S., and Schemm, S.: Jet Stream Dynamics from a Potential Vorticity Gradient Perspective: The Method and Its Application to a Kilometre-Scale Simulation, Quarterly Journal of the Royal Meteorological Society, 149, 2409–2432, https://doi.org/10.1002/qj.4513, 2023.

Cassou, C., Terray, L., and Phillips, A. S.: Tropical Atlantic Influence on European Heat Waves, Journal of Climate, 18, 2805–2811, https://doi.org/10.1175/JCLI3506.1, 2005.

Cattiaux, J., Peings, Y., Saint-Martin, D., Trou-Kechout, N., and Vavrus, S. J.: Sinuosity of Midlatitude Atmospheric Flow in a Warming World, Geophysical Research Letters, 43, 8259–8268, https://doi.org/10.1002/2016GL070309, 2016.

D'Andrea, F., Duvel, J.-P., Rivière, G., Vautard, R., Cassou, C., Cattiaux, J., Coumou, D., Faranda, D., Happé, T., Jézéquel, A., Ribes, A., and Yiou, P.: Summer Deep Depressions Increase Over the Eastern North Atlantic, Geophysical Research Letters, 51, e2023GL104 435, https://doi.org/10.1029/2023GL104435, 2024.

Davis, N. and Birner, T.: On the Discrepancies in Tropical Belt Expansion between Reanalyses and Climate Models and among Tropical Belt Width Metrics, https://doi.org/10.1175/JCLI-D-16-0371.1, 2017.

Davis, S. M. and Rosenlof, K. H.: A Multidiagnostic Intercomparison of Tropical-Width Time Series Using Reanalyses and Satellite Observations, https://doi.org/10.1175/JCLI-D-11-00127.1, 2012.

Di Capua, G. and Coumou, D.: Changes in Meandering of the Northern Hemisphere Circulation, Environmental Research Letters, 11, 094 028, https://doi.org/10.1088/1748-9326/11/9/094028, 2016.

Dima, I. M. and Wallace, J. M.: On the Seasonality of the Hadley Cell, 2003.

Francis, J. A. and Vavrus, S. J.: Evidence Linking Arctic Amplification to Extreme Weather in Mid-Latitudes, Geophysical Research Letters, 39, https://doi.org/10.1029/2012GL051000, 2012.

Francis, J. A. and Vavrus, S. J.: Evidence for a Wavier Jet Stream in Response to Rapid Arctic Warming, Environmental Research Letters, 10, 014 005, https://doi.org/10.1088/1748-9326/10/1/014005, 2015.

Franzke, C. and Woollings, T.: On the Persistence and Predictability Properties of North Atlantic Climate Variability, Journal of Climate, 24, 466–472, https://doi.org/10.1175/2010JCLI3739.1, 2011.

García-Burgos, M., Ayarzagüena, B., Barriopedro, D., and García-Herrera, R.: Jet Configurations Leading to Extreme Winter Temperatures Over Europe, Journal of Geophysical Research: Atmospheres, 128, e2023JD039 304, https://doi.org/10.1029/2023JD039304, 2023.

Geen, R., Thomson, S. I., Screen, J. A., Blackport, R., Lewis, N. T., Mudhar, R., Seviour, W. J. M., and Vallis, G. K.: An Explanation for the Metric Dependence of the Midlatitude Jet-Waviness Change in Response to Polar Warming, Geophysical Research Letters, 50, e2023GL105 132, https://doi.org/10.1029/2023GL105132, 2023.

Gibson, P. B., Perkins-Kirkpatrick, S. E., Uotila, P., Pepler, A. S., and Alexander, L. V.: On the Use of Self-Organizing Maps for Studying Climate Extremes, Journal of Geophysical Research: Atmospheres, 122, 3891–3903, https://doi.org/10.1002/2016JD026256, 2017.

Grams, C. M., Beerli, R., Pfenninger, S., Staffell, I., and Wernli, H.: Balancing Europe's Wind-Power Output through Spatial Deployment Informed by Weather Regimes, Nature Climate Change, 7, 557–562, https://doi.org/10.1038/nclimate3338, 2017.

Hannachi, A., Woollings, T., and Fraedrich, K.: The North Atlantic Jet Stream: A Look at Preferred Positions, Paths and Transitions, Quarterly Journal of the Royal Meteorological Society, 138, 862–877, https://doi.org/10.1002/qj.959, 2012.

Harnik, N., Galanti, E., Martius, O., and Adam, O.: The Anomalous Merging of the African and North Atlantic Jet Streams during the Northern Hemisphere Winter of 2010, Journal of Climate, 27, 7319–7334, https://doi.org/10.1175/JCLI-D-13-00531.1, 2014.

Harnik, N., Garfinkel, C. I., and Lachmy, O.: The Influence of Jet Stream Regime on Extreme Weather Events, in: Dynamics and Predictability of Large-Scale, High-Impact Weather and Climate Events, edited by Li, J., Swinbank, R., Grotjahn, R., and Volkert, H., pp. 79–94, Cambridge University Press, 1 edn., ISBN 978-1-107-77554-1 978-1-107-07142-1 978-1-107-41680-2, https://doi.org/10.1017/CBO9781107775541.007, 2016.

Harvey, B., Hawkins, E., and Sutton, R.: Storylines for Future Changes of the North Atlantic Jet and Associated Impacts on the UK, International Journal of Climatology, 43, 4424–4441, https://doi.org/10.1002/joc.8095, 2023.

Held, I. M.: Momentum Transport by Quasi-Geostrophic Eddies, Journal of the Atmospheric Sciences, 32, 1494–1497, https://doi.org/10.1175/1520-0469(1975)032<1494:MTBQGE>2.0.CO;2, 1975.

Held, I. M.: Large-Scale Dynamics and Global Warming, Bulletin of the American Meteorological Society, 74, 228–242, https://doi.org/10.1175/1520-0477(1993)074<0228:LSDAGW>2.0.CO;2, 1993.

Held, I. M. and Hou, A. Y.: Nonlinear Axially Symmetric Circulations in a Nearly Inviscid Atmosphere, Journal of the Atmospheric Sciences, 37, 515–533, https://doi.org/10.1175/1520-0469(1980)037<0515:NASCIA>2.0.CO;2, 1980.

Hersbach, H., Bell, B., Berrisford, P., Hirahara, S., Horányi, A., Muñoz-Sabater, J., Nicolas, J., Peubey, C., Radu, R., Schepers, D., Simmons, A., Soci, C., Abdalla, S., Abellan, X., Balsamo, G., Bechtold, P., Biavati, G., Bidlot, J., Bonavita, M., De Chiara, G., Dahlgren, P., Dee, D., Diamantakis, M., Dragani, R., Flemming, J., Forbes, R., Fuentes, M., Geer, A., Haimberger, L., Healy, S., Hogan, R. J., Hólm, E., Janisková, M., Keeley, S., Laloyaux, P., Lopez, P., Lupu, C., Radnoti, G., de Rosnay, P., Rozum, I., Vamborg, F., Villaume, S., and Thépaut, J.-N.: The ERA5 Global Reanalysis, Quarterly Journal of the Royal Meteorological Society, 146, 1999–2049, https://doi.org/10.1002/qj.3803, 2020.

Heskes, T.: Energy Functions for Self-Organizing Maps, in: Kohonen Maps, edited by Oja, E. and Kaski, S., pp. 303–315, Elsevier Science B.V., Amsterdam, ISBN 978-0-444-50270-4, https://doi.org/10.1016/B978-044450270-4/50024-3, 1999.

Hoskins, B. J. and Ambrizzi, T.: Rossby Wave Propagation on a Realistic Longitudinally Varying Flow, 1993.

Hoskins, B. J. and Hodges, K. I.: The Annual Cycle of Northern Hemisphere Storm Tracks. Part II: Regional Detail, Journal of Climate, 32, 1761–1775, https://doi.org/10.1175/JCLI-D-17-0871.1, 2019.

Huang, C. S. Y. and Nakamura, N.: Local Finite-Amplitude Wave Activity as a Diagnostic of Anomalous Weather Events, Journal of the Atmospheric Sciences, 73, 211–229, https://doi.org/10.1175/JAS-D-15-0194.1, 2016.

Jain, P. and Flannigan, M.: The Relationship between the Polar Jet Stream and Extreme Wildfire Events in North America, Journal of Climate, 34, 6247–6265, https://doi.org/10.1175/JCLI-D-20-0863.1, 2021.

Kållberg, P., Berrisford, P., Hoskins, B., Simmons, A., Uppala, S., Lamy-Thépaut, S., and Hine, R.: ERA-40 Atlas, Tech. Rep. 19, ECMWF, 2005.

Koch, P., Wernli, H., and Davies, H. C.: An Event-Based Jet-Stream Climatology and Typology, International Journal of Climatology, 26, 283–301, https://doi.org/10.1002/joc.1255, 2006.

Kohonen, T.: Self-Organized Formation of Topologically Correct Feature Maps, Biological Cybernetics, 43, 59–69, https://doi.org/10.1007/BF00337288, 1982.

Kohonen, T.: Essentials of the Self-Organizing Map, Neural Networks, 37, 52–65, https://doi.org/10.1016/j.neunet.2012.09.018, 2013.

Krishnamurti, T. N.: The Subtropical Jets Stream of Winter, Journal of the Atmospheric Sciences, 18, 172–191, https://doi.org/10.1175/1520-0469(1961)018<0172:TSJSOW>2.0.CO;2, 1961.

Lachmy, O.: The Relation Between the Latitudinal Shifts of Midlatitude Diabatic Heating, Eddy Heat Flux, and the Eddy-Driven Jet in CMIP6 Models, Journal of Geophysical Research: Atmospheres, 127, https://doi.org/10.1029/2022JD036556, 2022.

Lee, S. and Kim, H.-k.: The Dynamical Relationship between Subtropical and Eddy-Driven Jets, Journal of the Atmospheric Sciences, 60, 1490–1503, https://doi.org/10.1175/1520-0469(2003)060<1490:TDRBSA>2.0.CO;2, 2003.

Lin, L., Hu, C., Wang, B., Wu, R., Wu, Z., Yang, S., Cai, W., Li, P., Xiong, X., and Chen, D.: Atlantic Origin of the Increasing Asian Westerly Jet Interannual Variability, Nature Communications, 15, 2155, https://doi.org/10.1038/s41467-024-46543-x, 2024.

Maddison, J. W., Ayarzagüena, B., Barriopedro, D., and García-Herrera, R.: Added Value of a Multiparametric Eddy-Driven Jet Diagnostic for Understanding European Air Stagnation, Environmental Research Letters, 18, 084 022, https://doi.org/10.1088/1748-9326/ace72e, 2023.

Madonna, E., Li, C., Grams, C. M., and Woollings, T.: The Link between Eddy-Driven Jet Variability and Weather Regimes in the North Atlantic-European Sector, Quarterly Journal of the Royal Meteorological Society, 143, 2960–2972, https://doi.org/10.1002/qj.3155, 2017.

Maher, P., Kelleher, M. E., Sansom, P. G., and Methven, J.: Is the Subtropical Jet Shifting Poleward?, Climate Dynamics, 54, 1741–1759, https://doi.org/10.1007/s00382-019-05084-6, 2020.

Mahlstein, I., Martius, O., Chevalier, C., and Ginsbourger, D.: Changes in the Odds of Extreme Events in the Atlantic Basin Depending on the Position of the Extratropical Jet, Geophysical Research Letters, 39, https://doi.org/10.1029/2012GL053993, 2012.

Martin, J. E.: Recent Trends in the Waviness of the Northern Hemisphere Wintertime Polar and Subtropical Jets, Journal of Geophysical Research: Atmospheres, 126, e2020JD033 668, https://doi.org/10.1029/2020JD033668, 2021.

Martin, J. E. and Norton, T.: Waviness of the Southern Hemisphere Wintertime Polar and Subtropical Jets, Weather and Climate Dynamics, 4, 875–886, https://doi.org/10.5194/wcd-4-875-2023, 2023.

Martius, O.: A Lagrangian Analysis of the Northern Hemisphere Subtropical Jet, https://doi.org/10.1175/JAS-D-13-0329.1, 2014.

Martius, O. and Rivière, G.: Rossby Wave Breaking: Climatology, Interaction with Low-Frequency Climate Variability, and Links to Extreme Weather Events, in: Dynamics and Predictability of Large-Scale, High-Impact Weather and Climate Events, edited by Li, J., Swinbank,

R., Grotjahn, R., and Volkert, H., pp. 69–78, Cambridge University Press, 1 edn., ISBN 978-1-107-77554-1 978-1-107-07142-1 978-1-107-41680-2, https://doi.org/10.1017/CBO9781107775541.006, 2016.

Martius, O., Zenklusen, E., Schwierz, C., and Davies, H. C.: Episodes of Alpine Heavy Precipitation with an Overlying Elongated Stratospheric Intrusion: A Climatology, International Journal of Climatology, 26, 1149–1164, https://doi.org/10.1002/joc.1295, 2006.

Martius, O., Schwierz, C., and Davies, H. C.: Tropopause-Level Waveguides, Journal of the Atmospheric Sciences, 67, 866–879, https://doi.org/10.1175/2009JAS2995.1, 2010.

Michel, C. and Rivière, G.: The Link between Rossby Wave Breakings and Weather Regime Transitions, Journal of the Atmospheric Sciences, 68, 1730–1748, https://doi.org/10.1175/2011JAS3635.1, 2011.

Michelangeli, P.-A., Vautard, R., and Legras, B.: Weather Regimes: Recurrence and Quasi Stationarity, Journal of the Atmospheric Sciences, 52, 1237–1256, https://doi.org/10.1175/1520-0469(1995)052<1237:WRRAQS>2.0.CO;2, 1995.

Molnos, S., Mamdouh, T., Petri, S., Nocke, T., Weinkauf, T., and Coumou, D.: A Network-Based Detection Scheme for the Jet Stream Core, Earth System Dynamics, 8, 75–89, https://doi.org/10.5194/esd-8-75-2017, 2017.

Monahan, A. H. and Fyfe, J. C.: On the Nature of Zonal Jet EOFs, https://doi.org/10.1175/JCLI3960.1, 2006.

Nakamura, N. and Huang, C. S. Y.: Atmospheric Blocking as a Traffic Jam in the Jet Stream, Science, 361, 42–47, https://doi.org/10.1126/science.aat0721, 2018.

Palmen, E. and Newton, C. W.: A Study of the Mean Wind and Temperature Distribution in the Vicinity of the Polar Front in Winter, Journal of the Atmospheric Sciences, 5, 220–226, https://doi.org/10.1175/1520-0469(1948)005<0220:ASOTMW>2.0.CO;2, 1948.

Peings, Y., Cattiaux, J., Vavrus, S. J., and Magnusdottir, G.: Projected Squeezing of the Wintertime North-Atlantic Jet, Environmental Research Letters, 13, 074 016, https://doi.org/10.1088/1748-9326/aacc79, 2018.

Pena-Ortiz, C., Gallego, D., Ribera, P., Ordonez, P., and Alvarez-Castro, M. D. C.: Observed Trends in the Global Jet Stream Characteristics during the Second Half of the 20th Century, Journal of Geophysical Research: Atmospheres, 118, 2702–2713, https://doi.org/10.1002/jgrd.50305, 2013.

Röthlisberger, M., Martius, O., and Wernli, H.: An Algorithm for Identifying the Initiation of Synoptic-Scale Rossby Waves on Potential Vorticity Waveguides, Quarterly Journal of the Royal Meteorological Society, 142, 889–900, https://doi.org/10.1002/qj.2690, 2016a.

Röthlisberger, M., Pfahl, S., and Martius, O.: Regional-Scale Jet Waviness Modulates the Occurrence of Midlatitude Weather Extremes: Jet waviness and weather extremes, Geophysical Research Letters, 43, 10,989–10,997, https://doi.org/10.1002/2016GL070944, 2016b.

Rousi, E., Kornhuber, K., Beobide-Arsuaga, G., Luo, F., and Coumou, D.: Accelerated Western European Heatwave Trends Linked to More-Persistent Double Jets over Eurasia, Nature Communications, 13, 3851, https://doi.org/10.1038/s41467-022-31432-y, 2022.

Sato, Y., Nakajima, S., Shiraga, N., Atsumi, H., Yoshida, S., Koller, T., Gerig, G., and Kikinis, R.: Three-Dimensional Multi-Scale Line Filter for Segmentation and Visualization of Curvilinear Structures in Medical Images, Medical Image Analysis, 2, 143–168, https://doi.org/10.1016/s1361-8415(98)80009-1, 1998.

Schneider, E. K.: Axially Symmetric Steady-State Models of the Basic State for Instability and Climate Studies. Part II. Nonlinear Calculations, Journal of the Atmospheric Sciences, 34, 280–296, https://doi.org/10.1175/1520-0469(1977)034<0280:ASSSMO>2.0.CO;2, 1977.

Shaw, T. A. and Miyawaki, O.: Fast Upper-Level Jet Stream Winds Get Faster under Climate Change, Nature Climate Change, 14, 61–67, https://doi.org/10.1038/s41558-023-01884-1, 2024.

Spensberger, C., Spengler, T., and Li, C.: Upper-Tropospheric Jet Axis Detection and Application to the Boreal Winter 2013/14, Monthly Weather Review, 145, 2363–2374, https://doi.org/10.1175/MWR-D-16-0467.1, 2017.

Spensberger, C., Li, C., and Spengler, T.: Linking Instantaneous and Climatological Perspectives on Eddy-Driven and Subtropical Jets, Journal of Climate, 36, 8525–8537, https://doi.org/10.1175/JCLI-D-23-0080.1, 2023.

Stendel, M., Francis, J., White, R., Williams, P. D., and Woollings, T.: The Jet Stream and Climate Change, in: Climate Change, pp. 327–357, Elsevier, ISBN 978-0-12-821575-3, https://doi.org/10.1016/B978-0-12-821575-3.00015-3, 2021.

Stryhal, J. and Plavcová, E.: On Using Self-Organizing Maps and Discretized Sammon Maps to Study Links between Atmospheric Circulation and Weather Extremes, International Journal of Climatology, 43, 2678–2698, https://doi.org/10.1002/joc.7996, 2023.

Totz, S., Petri, S., Lehmann, J., and Coumou, D.: Regional Changes in the Mean Position and Variability of the Tropical Edge, Geophysical Research Letters, 45, 12,076–12,084, https://doi.org/10.1029/2018GL079911, 2018.

Tuel, A. and Martius, O.: Weather Persistence on Sub-Seasonal to Seasonal Timescales: A Methodological Review, Earth System Dynamics, 14, 955–987, https://doi.org/10.5194/esd-14-955-2023, 2023.

Vallis, G. K.: Atmospheric and Oceanic Fluid Dynamics: Fundamentals and Large-Scale Circulation, Cambridge University Press, 2 edn., ISBN 978-1-107-06550-5 978-1-107-58841-7, https://doi.org/10.1017/9781107588417, 2017.

Weiland, R. S., van der Wiel, K., Selten, F., and Coumou, D.: Intransitive Atmosphere Dynamics Leading to Persistent Hot–Dry or Cold–Wet European Summers, Journal of Climate, 34, 6303–6317, https://doi.org/10.1175/JCLI-D-20-0943.1, 2021.

White, R. H.: Time-Varying Atmospheric Waveguides – Climatologies and Connections to Quasi-Stationary Waves, EGUsphere, pp. 1–21, https://doi.org/10.5194/egusphere-2024-966, 2024.

Winters, A. C. and Martin, J. E.: Diagnosis of a North American Polar–Subtropical Jet Superposition Employing Piecewise Potential Vorticity Inversion, Monthly Weather Review, 145, 1853–1873, https://doi.org/10.1175/MWR-D-16-0262.1, 2017.

Winters, A. C., Keyser, D., Bosart, L. F., and Martin, J. E.: Composite Synoptic-Scale Environments Conducive to North American Polar–Subtropical Jet Superposition Events, Monthly Weather Review, 148, 1987–2008, https://doi.org/10.1175/MWR-D-19-0353.1, 2020.

Wirth, V.: Waveguidability of Idealized Midlatitude Jets and the Limitations of Ray Tracing Theory, Weather and Climate Dynamics, 1, 111–125, https://doi.org/10.5194/wcd-1-111-2020, 2020.

Wirth, V. and Polster, C.: The Problem of Diagnosing Jet Waveguidability in the Presence of Large-Amplitude Eddies, Journal of the Atmospheric Sciences, 78, 3137–3151, https://doi.org/10.1175/JAS-D-20-0292.1, 2021.

Woollings, T., Hannachi, A., and Hoskins, B.: Variability of the North Atlantic Eddy-Driven Jet Stream: Variability of the North Atlantic Jet Stream, Quarterly Journal of the Royal Meteorological Society, 136, 856–868, https://doi.org/10.1002/qj.625, 2010.

Woollings, T., Czuchnicki, C., and Franzke, C.: Twentieth Century North Atlantic Jet Variability, Quarterly Journal of the Royal Meteorological Society, 140, 783–791, https://doi.org/10.1002/qj.2197, 2014.

Woollings, T., Barnes, E., Hoskins, B., Kwon, Y.-O., Lee, R. W., Li, C., Madonna, E., McGraw, M., Parker, T., Rodrigues, R., Spensberger, C., and Williams, K.: Daily to Decadal Modulation of Jet Variability, Journal of Climate, 31, 1297–1314, https://doi.org/10.1175/JCLI-D-17-0286.1, 2018a.

Woollings, T., Barriopedro, D., Methven, J., Son, S.-W., Martius, O., Harvey, B., Sillmann, J., Lupo, A. R., and Seneviratne, S.: Blocking and Its Response to Climate Change, Current Climate Change Reports, 4, 287–300, https://doi.org/10.1007/s40641-018-0108-z, 2018b.

Woollings, T., Drouard, M., O'Reilly, C. H., Sexton, D. M. H., and McSweeney, C.: Trends in the Atmospheric Jet Streams Are Emerging in Observations and Could Be Linked to Tropical Warming, Communications Earth & Environment, 4, 1–8, https://doi.org/10.1038/s43247-023-00792-8, 2023.